Chemical Geology 639 (2023) 121715

Contents lists available at ScienceDirect

Chemical Geology

journal homepage: www.elsevier.com/locate/chemgeo

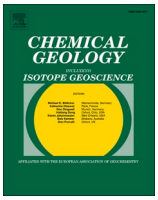

Lead isotopes and rare earth elements geochemistry of global phosphate rocks: Insights into depositional conditions and environmental tracing

Zhen Wang [a], Robert Hill [a], Gordon Williams [a], Gary S. Dwyer [a], Jun Hu [a], Ewald Schnug [b], Roland Bol [c], Yajie Sun [c,d], Drew S. Coleman [e], Xiao-Ming Liu [e], Michael R. Sandstrom [e], Avner Vengosh [a,*]

[a] Nicholas School of the Environment, Duke University, Durham, NC 27708, USA
[b] Faculty of Life Sciences, Technical University, Universitätsplatz 2, Braunschweig D-38106, Germany
[c] Institute of Bio- and Geosciences: Agrosphere (IBG-3), Forschungszentrum Jülich GmbH, Jülich 52425, Germany
[d] University of Bonn, Institute of Crop Science and Resource Conservation, Soil Science and Soil Ecology, Nussallee 13, Bonn 53115, Germany
[e] Department of Earth, Marine and Environmental Sciences, The University of North Carolina at Chapel Hill, Chapel Hill, NC 27599, USA

ARTICLE INFO

Editor: Christian France-Lanord

Keywords:
Pb isotopes
Rare earth elements
Phopshate rocks
Depositional conditions
Phosphate fertilizers
Environmental tracing

ABSTRACT

Phosphate rock bears both geologically and environmentally significant information. Rare earth elements and yttrium (i.e., REY) characteristics have been commonly used for reconstructing the redox conditions of depositional environments and the effects of post-depositional diagenetic alteration on phosphate rock. In addition, phosphate rock is typically enriched in a range of trace elements such as uranium (U) and cadium (Cd) that can be dispersed as contaminants into the environment with phosphate mining and phosphate fertilizer application. Here we report the lead (Pb) isotope compositions combined with Pb and REY concentrations of both global sedimentary and igneous phosphate rocks, aiming to evalute the geological origin of phosphate rocks over time and the potential of using them for environmental tracing. Phopshate rock samples analyzed in this study were sourced from major economic phosphate deposits in the world, including China, Southern Tethys (e.g., Morocco, Tunisia, Israel), the U.S., India, South Africa and Russia. Our results show a wide range of $^{208}Pb/^{204}Pb$ (35.70 to 60.58), $^{207}Pb/^{204}Pb$ (15.20 to 18.25), and $^{206}Pb/^{204}Pb$ (16.369 to 71.806) ratios in the phosphate rocks, with sedimentary phosphate rocks being significantly more radiogenic than igneous rocks. The majority of sedimentray phosphate rocks show a notable isotopic overprinting by non-radiogenic terrestrial Pb, except for those from Israel and Morocco that have the most radiogenic Pb isotope compositions. Correspondingly, phosphate rocks with more radiogenic Pb isotope ratios show relatively pristine seawater REY features, likely suggesting their preservation of the original oxic seawater conditions and/or minimal diagenetic alteration. In contrast, phosphate rocks with less radiogenic Pb isotope compositions show REY indications for more anoxic seawater redox conditions and/or greater diagenetic alteration. We further evaluate the potential utility of Pb isotopes for tracing the associated contamination with phosphate rock mining and fertilizer application in the environment. In most cases, the radiogenic Pb isotope composition of phosphate rocks and corresponding P-fertilizers is distinctive from both natural crustal Pb and major anthropogenic Pb sources (e.g., Pb ore deposits and pesticides), which provides a great advantage for applying Pb isotopes as an environmental tracer for metal(loid) contamination from phosphate sources. The combination of Pb isotope ratios and REY proxies could further constrain the Pb source discrimination. Overall, this study provides new Pb isotopic and REY geochemical data on global phosphate rocks and fertilizers, which lays the groundwork for future regional and local studies on both their geological and environmental implications.

1. Introduction

Phosphate rock is the most important source for phosphorus (P), which is an essential nutrient element for both agricultural (Schnug and De Kok, 2016) and industrial applications (Filippelli, 2011; Pufahl and Groat, 2017). Marine sedimentary phosphate deposits represent the

* Corresponding author.
E-mail address: vengosh@duke.edu (A. Vengosh).

https://doi.org/10.1016/j.chemgeo.2023.121715
Received 14 May 2023; Received in revised form 30 August 2023; Accepted 6 September 2023
Available online 9 September 2023

majority of the global phosphate resources, accounting for approximately 95% of the global total, while igneous phosphate deposits represent about 5% (Cook and Shergold, 2005; Notholt et al., 2005; Pufahl and Groat, 2017). While the mineralogical composition of marine sedimentary phosphate is dominantly composed of carbonate fluorapatite (i.e., CFA) (McClellan, 1980; Pufahl and Groat, 2017), large compositional variations of phosphate rocks are often observed (e.g., via progressive decarbonation and elemental substitutions in phosphate rock through geological time) (McClellan and Van Kauwenbergh, 1991). The large chemical variations observed in phosphate rocks can be attributed to the complex nature of phosphate sedimentation and the combined effects of original depositional environments, early- and post-depositional diagenetic alteration, physical reworking after deposition, weathering, and metamorphism over time (McClellan and Van Kauwenbergh, 1991; Van Kauwenbergh et al., 1990).

Rare earth elements and yttrium (i.e., REE + Y or derfined as REY) have similar ionic radii to calcium (Ca), and therefore are preferentially incorporated into phosphates via substitution for Ca in the crystal lattice of phosphate minerals (e.g., apatite $Ca_5(PO_4)_3(F,Cl,OH)$) (Auer et al., 2017; Emsbo et al., 2015; Garnit et al., 2012; German and Elderfield, 1990). As a result, phosphate rock generally contains considerable amounts of REY and, thus, becomes an important resource for REY of potential economic significance (El Bamiki et al., 2021; Emsbo et al., 2016; Emsbo et al., 2015). Furthermore, due to their distribution and fractionation characteristics, REY have been widely used as proxies to characterize the paleoenvironmental conditions of phosphate formation and post-depositional diagenetic influences on marine sedimentary phosphates (Auer et al., 2017; Garnit et al., 2012; McArthur and Walsh, 1984; Shields and Stille, 2001; Yang et al., 2022, Yang et al., 2019; references therein).

In addition to REY, phosphate rock is enriched in various trace elements, including uranium (U) (Fayiga and Nwoke, 2016; Pufahl and Groat, 2017; Schnug et al., 2023). Consequently, previous studies have utilized the U—Pb and Pb—Pb geochronology for age-dating of sedimentary phosphates (Aubineau et al., 2022; Chen et al., 2004; O'Sullivan et al., 2021). However, attempts to use Pb isotopes for tracing phosphate-related contamination in the environment are limited. A few studies have shown the distinctive radiogenic Pb isotope ratios in phosphate rocks and phosphate fertilziers. For example, Roy and Négrel (2001) found that the Pb isotope ratios (e.g., $^{206}Pb/^{204}Pb$) of a few phosphate fertilizers were notably higher than those of the other natural and anthropogenic sources in the area of Massif Central (France). Abi-Ghanem et al. (2009) demonstrated that the Lebanese coastal sediments from a site impacted by phosphogypsum discharge exhibited exceptionally radiogenic Pb isotope compositions as compared to the Pb ratios in non-impacted sediments. Kamenov et al. (2009) reported Pb isotope ratios of a few phosphate rocks from Florida, which were also distinctively more radiogenic than other natural and anthropogenic Pb sources, thus excluding the possible impacts of phosphate mining activities in the history of peat sediments characterized by less radiogenic Pb ratios. Yet, there is a paucity of published data on the Pb isotope compositions of phosphate rocks of diverse geological ages and from various geographic regions around the globe.

The environmental impacts associated with the dissolution of phosphate rocks include the release of toxic metals such as U and cadmium (Cd), as well as radionuclides from the ^{238}U decay series (Fayiga and Nwoke, 2016; Pufahl and Groat, 2017; Schnug et al., 2023). These contaminants tend to remain enriched in phosphate mining wastes (Gnandi and Tobschall, 1999; Vengosh et al., 2022), phosphate fertilizers, and gypsum byproducts (Aoun et al., 2010; Gaudry et al., 2007; Martínez-Aguirre et al., 1994; Pérez-López et al., 2010; Rutherford et al., 1994; Sattouf et al., 2008; Sattouf et al., 2007; Verbeeck et al., 2020). The partitioning of elements between phosphate rock and its (by) products varies considerably depending on rock sources and production processes (Rutherford et al., 1995; Sattouf et al., 2008; Sattouf et al., 2007), which may limit the ability of using element enrichment alone for identifying the related contamination. It has been suggested using different geochemical and isotopic tracers such as Sr isotopes for detecting phosphate mining wastes in the environment (Vengosh et al., 2022). Yet, due to the potential overlap of geochemical signals between the phosphate rock and natural background and/or other anthropogenic sources, additional tracers are needed to obtain reliable information of possible environmental impacts from phosphate rock mining and phosphate fertilizers utilization.

Here we present the first set of Pb concentrations and isotopes data as well as new REY data on phosphate rocks originating from the major economic phosphate deposits worldwide. Phosphate rock samples analyzed in this study were formed over a wide range of geological ages from the late Paleoproterozoic to the middle Miocene, and across diverse settings and geographic regions, including those of marine sedimentary type from the Southern Tethys (i.e., North Africa and the Middle East), Eastern U.S., China, and India, as well as igneous phosphate rocks from Russia, Brazil, and South Africa (Pufahl and Groat, 2017; Sun et al., 2020). The main objectives of this study are (1) to characterize the Pb concentrations and isotope compositions combined with REY variations of bulk phosphate rocks of different geological ages and geographic regions; (2) to reconstruct possible depositional conditions and diagenetic alteration based on the Pb isotope and REY geochemistry variations in phosphate rocks; and (3) to assess the potential of using Pb isotope ratios in combination with REY proxies for environmental tracing through systematic charactarization of the geochemical signatures of phosphate fertilizers and phosphate rocks, in comparison to Pb isotope composition of other anthropogenic Pb sources.

2. Methods

2.1. Sample collection

As shown in the Appendix A Supplementary data (Table S1), the regions of origin for the phosphate rock samples analyzed in this study include the USA ($n = 5$), Peru ($n = 1$), Brazil ($n = 2$), the western Sahara ($n = 1$), Senegal ($n = 2$), Togo ($n = 3$), South Africa ($n = 2$), Algeria (n = 2), Tunisia (n = 3), Morocco ($n = 4$), Israel ($n = 7$), Syria (n = 2), Jordan (n = 1), Egypt (n = 2), China ($n = 14$), India ($n = 5$), and Russia (n = 2). The types of analyzed phosphate rock samples include marine sedimentary ($n = 49$), igneous ($n = 8$), and metamorphic (n = 1). The ages of the sedimentary phosphate rock samples span from the late Paleoproterozoic (~ 1900 Ma) to the mid Miocene (~ 13 Ma) (Sun et al., 2020). The North African and Middle Eastern phosphate rocks were mostly sourced from the late Cretaceous-Eocene South Tethyan phosphogenic province, which is the largest accumulation of phosphate on Earth, hosting over 85% of the world's known phosphate reserves (Pufahl and Groat, 2017). The majority of the Chinese phosphate rocks originated from the late Neoproterozoic Duoshantuo Formation in South China, which contains 5% of the global reserves and yet accounts for 45% of the world's current phosphate production (Pufahl and Groat, 2017). The U.S. phosphate rocks were derived from the middle Miocene Hawthorn Group in Florida and associated deposits in North Carolina, representing 80% of phosphate production in the U.S. (Pufahl and Groat, 2017). The igneous samples were mainly from the Khibina Alkaline Complex in Russia's Kola Peninsula, which is the world's largest igneous source of phosphate rock, accounting for 58% of all the igneous phosphate rock production, followed by the alkaline carbonatite complexes of Brazil (31%), and the Phalabora complex in South Africa (10%) (Pufahl and Groat, 2017).

In addition to phosphate rocks, several phosphate fertilizer samples of various types (i.e., triple super phosphate (TSP), single super phosphate (SSP), di-ammonium phosphate fertilizer (DAP), and phosphate potassium fertilizer (PK)) were collected and analyzed from the corresponding phosphate-producing countries, including USA ($n = 4$), China (n = 4), Israel ($n = 3$), Morocco ($n = 1$), Jordan (n = 1), and India (n = 1) (Table S2).

2.2. Sample preparation

Digestion of whole-rock phosphate and fertilizer samples for both elemental and isotope analysis was performed using concentrated hydrofluoric (HF) and nitric (HNO_3) acids ($v/v = 2:1$; optima grade, Fisher Chemical™) heated at 105 °C for 24 h in sealed Teflon beakers. Following that, the solution was dried at 105 °C in open beakers and then brought back to solution in a mixture of HNO_3 (1 mL; optima grade, Fisher Chemical™), H_2O_2 (1 mL; optima grade, Fisher Chemical™), and deionized (DI) water (5 mL). The efficiency of digestion and accuracy of measurement are assessed by repetitively measuring the Natural Moroccan Phosphate Rock BCR-032 from the European Commission Joint Research Center Institute for Reference Materials and Measurements (IRMM).

For the purpose of comparison, selective extraction of carbonate-fluorapatite (CFA) from bulk phosphate rock was applied to select samples using a modified method based on previous studies (Abouzeid and El-Jallad, 1980; Soudry et al., 2006). Specifically, the sample was first calcined at 750 °C for 1 h in a muffle furnace, rinsed with deionized (DI) water 3 times, and dried in an oven at 50 °C for 24 h. An aliquot of the calcined sample was then treated with 0.5 M tri-ammonium citrate (TAC) solution (pH = 8) at a 10:1 mL/g liquid to solid ratio and shaken at room temperature for 24 h. Following the TAC leach, the residue was separated using a centrifuge and DI-rinsed and oven-dried at 50 °C. The separated residue (i.e., carbonate-fluorapatite fraction) was leached with 0.5 M HNO_3.

2.3. Elemental analysis

Rare earth elements and yttrium (REY) as well as Al, Pb, Th, and U in the digested whole-rock samples and extracted CAF samples were measured on an inductively coupled plasma mass spectrometer (ICP-MS, Thermo Fisher X-Series II) at Duke University, equipped with a collision/reaction cell device. Note that Tm was not included in the analytes, due to its presence in the internal standard mixture (In, Tm, and Bi) spiked for the ICP-MS analysis. Measured REY concentrations were normalized to their respective concentrations in the Post-Archean Australian Shale (PAAS) (Nance and Taylor, 1976), denoted as $[REY]_N$ hereafter. The REY indices (e.g., Ce/Ce*) were all calculated using the PAAS-normalized values. A three-fold classification for REY was adopted in this study, namely light REY (i.e., La, Ce, Pr, Nd, and Sm), middle REY (i.e., Eu. Gd, Tb, Dy, and Y), and heavy REY (i.e., Ho, Er, Yb, and Lu).

2.4. Pb isotope analysis

The Pb isotope ratios (i.e., $^{208}Pb/^{204}Pb$, $^{206}Pb/^{204}Pb$, $^{207}Pb/^{204}Pb$, $^{208}Pb/^{206}Pb$, and $^{206}Pb/^{207}Pb$) of the prepared phosphate rock and fertilizer samples were measured on a high-resolution thermal ionization mass spectrometer (TIMS, Thermo Fisher Triton) at Duke University, equipped with Faraday cups and operated in static mode. A common Pb standard NIST SRM 981 was measured regularly over the course of analysis ($n = 31$) and the average mass bias of 0.14%/amu for all isotope ratios was determined according to the respective isotope ratios reported by Yuan et al. (2016). The average analytical uncertainties (2SD) are 0.03 for $^{208}Pb/^{204}Pb$, 0.01 for $^{207}Pb/^{204}Pb$, 0.008 for $^{206}Pb/^{204}Pb$, 0.0008 for $^{208}Pb/^{206}Pb$, and 0.0002 for $^{206}Pb/^{207}Pb$. A handful of fertilizer samples (i.e., CNPF_1, CNPF_2, CNPF_3, and CNPF_4; Table S2) were measured on an IsotopX Phoenix X62 TIMS in the Isotope Geochemistry Lab at the University of North Carolina at Chapel Hill. The data were also corrected with 0.14%/amu for fractionation. The Pb column separation and purification procedures are detailed elsewhere (Wang et al., 2019).

2.5. X-ray diffraction (XRD) analysis

Select phosphate rock samples were analyzed by powder X-ray diffraction (XRD) in the Shared Materials Instrumentation Facility (SMIF) at Duke University. Analysis was performed on a Panalytical X'Pert PRO MRD HR diffractometer with Cu Kα radiation and operated at 45 kV and 40 mA with a ½ degree fixed divergent slit, 10 mm beam mask, and 0.04 rad soller slit. Data collection ranged from 10° to 80° (2θ) with a 0.05° step size and a 3° per minute scan rate. In preparation for analysis, powdered samples were secured onto an amorphous glass slide with double sided tape.

2.6. Calculations and statistics

All statistical calculations and analyses were performed in R (v 4.1.1) (R Core Team, 2021). Nonparametric analyses were conducted, including Mann-Whitney test and Spearman's rank correlation test where Rho (ρ) = 1, −1, and 0 indicate total positive, total negative, and no correlation, repsectively. Statistical significance is based on p value, where $p < 0.01$ for 99% confidence interval and $p < 0.05$ for 95% confidence interval.

3. Results

3.1. Pb concentration and isotope composition

Phosphate rocks of different rock types, geological ages, and geographic regions display large variations in Pb concentrations and isotope compositions (Table S1; Fig. 1). The Pb concentrations in younger sedimentary phosphate rocks (i.e., late Cretaceous – middle Miocene; 0.88–12.8 mg/kg) are significantly lower than that of older phosphate rocks (e.g., Precambrian – late Devonian; 1.59–187 mg/kg) ($p = 3.2 \times 10^{-5}$), and there is no significant difference ($p = 0.57$) between sedimentary and igneous rocks in Pb concentrations (Table S1; Fig. 1A). The Pb isotope composition of all the bulk phosphate rock samples analyzed in this study shows a wide range from 35.70 to 60.58 for $^{208}Pb/^{204}Pb$, 15.20 to 18.25 for $^{207}Pb/^{204}Pb$, and 16.369 to 71.806 for $^{206}Pb/^{204}Pb$ (Table S1). Generally, sedimentary phosphate rocks have more radiogenic Pb (i.e., higher $^{206}Pb/^{204}Pb$ and $^{207}Pb/^{204}Pb$ ratios) than those of igneous type ($p = 5.5 \times 10^{-5}$) (Figs. 1 and 2). The highest $^{207}Pb/^{204}Pb$ and $^{206}Pb/^{204}Pb$ ratios in sedimentary phosphate rocks are 18.25 and 71.806, respectively, compared to the maximum ratios of 16.07 for $^{207}Pb/^{204}Pb$ and 27.778 for $^{206}Pb/^{204}Pb$ in igneous rock samples (Table S1; Figs. 1 and 2). The two igneous phosphate rocks from Russia, particularly, have a distinct thorogenic composition (i.e., high $^{208}Pb/^{204}Pb$ ratios varying from 57.60 to 60.58) (Table S1; Fig. 1A and B), which are notably divergent from the array defined by the rest of samples on the plot of $^{208}Pb/^{206}Pb$ vs. $^{206}Pb/^{207}Pb$ (Fig. 2D). The Pb isotope compositions of igneous rock samples from China, Brazil, and South Africa are among the least radiogenic ratios compared to the igneous samples from Russia and many of the sedimentary phosphate rock samples (Table S1; Figs. 1 and 2).

In spite of the large difference in Pb concentrations, there is no specific trend in the Pb isotope compositions of the sedimentrary phosphate rocks over geological time (Fig. 1B-C). In general, the Pb isotope compositions of younger sedimentary phosphate rocks (i.e., late Cretaceous – middle Miocene) are significantly more radiogenic than that of older phosphate rocks (e.g., Precambrian – late Devonian) ($p = 0.0004$; Table S1; Fig. 1B-C). Among the younger phosphate rocks, those from the eastern U.S. and Peru have the least uranogenic compositions (i.e., lowest $^{207}Pb/^{204}Pb$ and $^{206}Pb/^{204}Pb$ ratios). The oldest phosphate rocks from India (i.e., late Paleoproterozoic) are less radiogenic in Pb isotope compositions compared to the late Neoproterozoic and early Cambrian ones from China (Table S1; Figs. 1 and 2).

Among all of the analyzed sedimentary phosphate rocks, the southern Tethyan samples from North Africa and Middle East have the highest

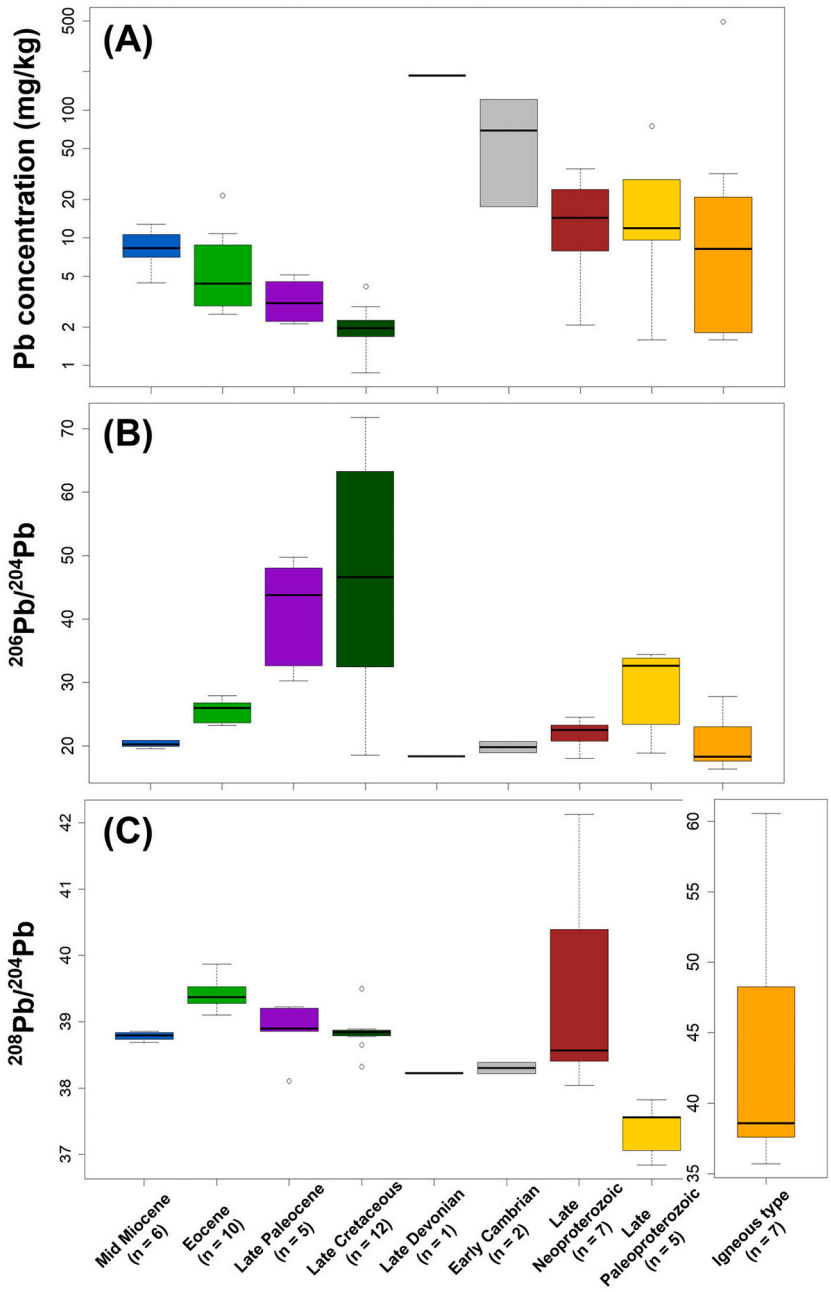

Fig. 1. Boxplots showing distribution of Pb concentrations (A) and Pb isotope compositions $^{206}Pb/^{204}Pb$ (B) and $^{208}Pb/^{204}Pb$ (C) in sedimentary phosphate rock samples sorted by geological age as well as igneous phosphate rock samples analyzed in this study (Table S1).

radiogenic isotopic ratios compared to phosphate rocks from the other regions ($p = 2.0 \times 10^{-5}$; Table S1; Fig. 2). Of the southern Tethyan samples, those originating from Israel have the highest $^{207}Pb/^{204}Pb$ and $^{206}Pb/^{204}Pb$ ratios, averaging at 17.57 and 58.272, respectively, followed by samples from Morocco, Syria, Jordan, Egypt, Western Sahara, Tunisia, Senegal, Algeria, and Togo (Table S1; Fig. 2). In comparison, phosphate rocks from the U.S. have notably less radiogenic isotope ratios for $^{207}Pb/^{204}Pb$ (mean = 15.73) and $^{206}Pb/^{204}Pb$ (mean = 20.444) (Table S1), which are close to the values previously reported for the four phosphorites from Florida (Kamenov et al., 2009). Phosphate rocks from China have an isotopic range of 15.20–16.21 and 16.369–24.538 for $^{207}Pb/^{204}Pb$ and $^{206}Pb/^{204}Pb$, respectively (Table S1). The ratios of those Precambrian samples are within the reported Pb isotope range for the Neoproterozoic phosphorites in South China (Chen et al., 2004). In comparison, the isotopic range of the older phosphate rocks from India is wider (i.e., 15.81–17.19 for $^{207}Pb/^{204}Pb$ and 18.890–34.395 for $^{206}Pb/^{204}Pb$; Table S1).

The qualitative and semi-quantitative analyses of the minerlogical composition of select phosphate rocks show that most of the young sedimentrary phosphate rocks (i.e., those from the eastern U.S., Peru, Senegal, Israel, and Morocco) are composed of primarily carbonate fluorapatite or CFA (i.e., 80–100% with an exception of IL_1 having 55%; Figs. S4 and S5), whereas older samples from China and India contain lower percentages of CFA (i.e., 40–79% with an exception of IN_1 containing 99%; Figs. S3 and S4). In addition to the bulk phosphate rocks, we analyzed the Pb concentrations and isotope ratios of extracted carbonate-fluorapatite (CFA) phase for select phosphate rocks samples (Table S3; Figs. S1 and S2), in particular those with relatively low percentage of CFA phase in the bulk phosphate rocks (e.g., China and India; Figs. S3 and S4). The results show that the proportions of Pb in the

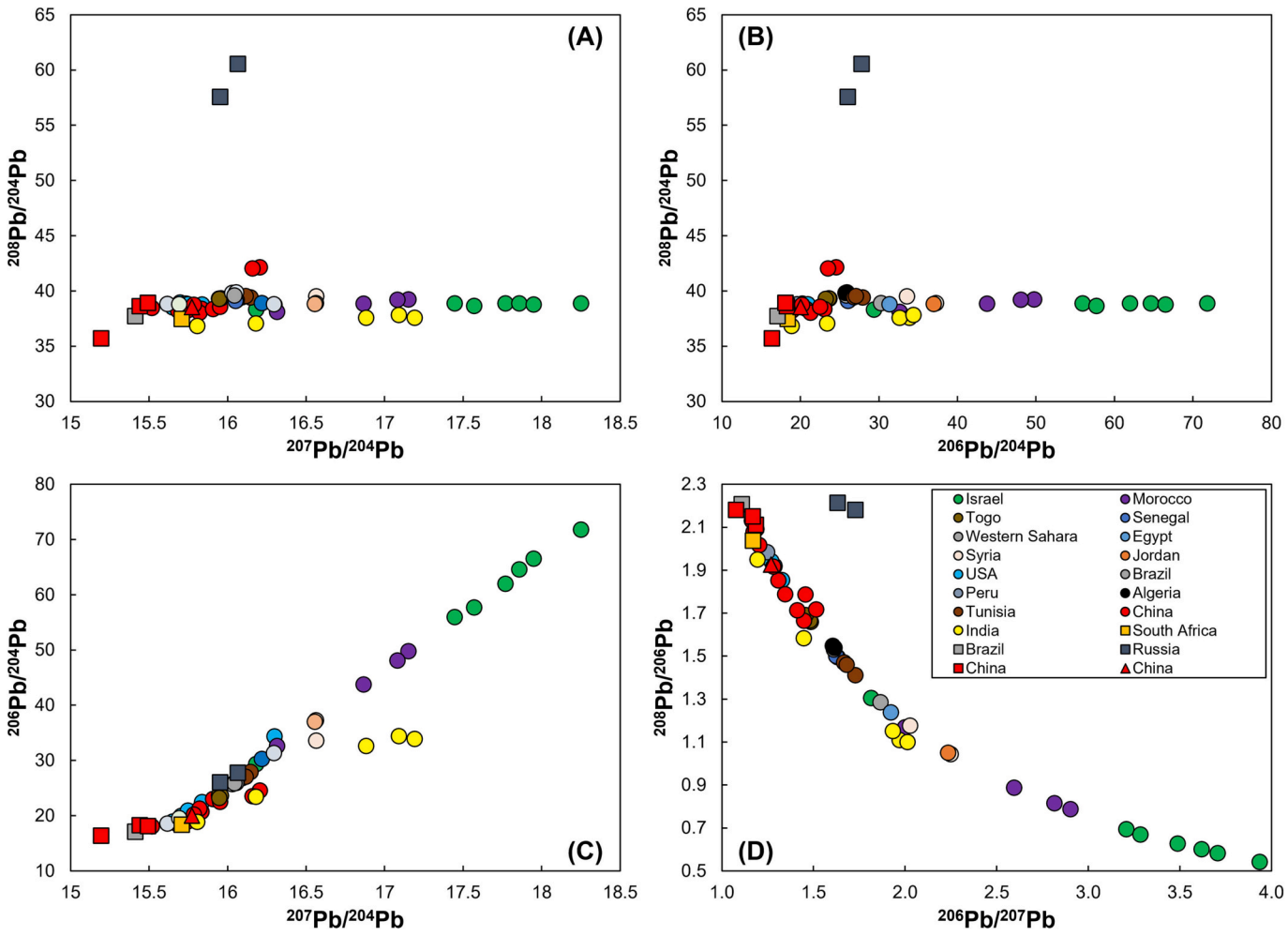

Fig. 2. Binary scatter plots of Pb isotopes ratios for all phosphate rock samples analyzed in this study. (A) $^{208}Pb/^{204}Pb$ vs. $^{207}Pb/^{204}Pb$. (B) $^{208}Pb/^{204}Pb$ vs. $^{206}Pb/^{204}Pb$. (C) $^{206}Pb/^{204}Pb$ vs. $^{207}Pb/^{204}Pb$. (D) $^{208}Pb/^{206}Pb$ vs. $^{206}Pb/^{207}Pb$. Circle, square, and triangle symbols refer to marine sedimentary, igneous, and metamorphic types of phosphate rocks, respectively.

extracted CFA phase relative to the bulk phosphate rock range from 12% to 59% (38% on average, $n = 11$; Fig. S1), indicating that the non-CFA phases in the phosphate rock can contribute a significant amount of Pb. However, the Pb isotope ratios of the CFA phase are not significantly different from the respective bulk rock ratios ($p = 0.95$), and follow the same array on the plot of $^{208}Pb/^{206}Pb$ vs. $^{206}Pb/^{207}Pb$ (Table S3; Fig. S2). This suggests Pb isotope compsotion of the bulk phosphate rocks reflects both the CFA phase and other co-occuring minerals in the phosphate rocks.

3.2. Rare earth elements and Y (REY)

The total concentration of REY in the analyzed phosphate rock samples of sedimentary type (mean = 329 mg/kg) is significantly lower than that of igneous type samples (mean = 3809 mg/kg) ($p = 0.001$; Table S1), which is consistent with results reported in previous studies (El Bamiki et al., 2021). Sedimentary phosphate rocks have a total REY ranging from 17 to 1060 mg/kg, whereas the total REY of igneous samples is up to 6000 mg/kg (Table S1). There is no significant correlation between the total REY and age of sedimentary phosphate rocks analyzed in this study (Fig. S6A), although it appears that samples of younger age (i.e., late Cretaceous – mid Miocene) from the U.S and South Tethys have higher total REY concentrations than those of older (i.e., Precambrian – late Devonian) phosphate rocks from China and India. This contrasts with previous suggestion that total REY concentrations in phosphate rocks generally increase with geological age (McArthur and Walsh, 1984). The REY concentrations of extracted carbonate-fluorapatite (CFA) phase for select phosphate rocks samples show its predominant contribution to the total REY in phosphate rock (i.e., ranging from 57% to 98% with an average of 80%, $n = 11$); therefore, the REY composition in the phosphate rocks directly reflects the CFA phase, even in rocks with relatively low percent of CFA (Table S3).

The binary plots of $[La]_N/[Yb]_N$ vs. total REY and $[La]_N/[Yb]_N$ vs. $[Y]_N/[Ho]_N$ clearly separate the sedimentary from the igneous phosphate rock samples, while the one metamorphic sample from China is within the compositional field of sedimentary rocks (Fig. 3). In general, the REY composition of sedimentary phosphate rocks is characterized by the depletion of light REY (i.e., $[La]_N/[[Yb]_N < 1$, $[Pr]_N/[Yb]_N < 1$), negative Ce anomalies (i.e., $Ce/Ce^* < 1$; $Ce/Ce^* = 2[Ce]_N/([La]_N+[Nd]_N)$ (Bau and Dulski, 1996)), no Eu anomalies (i.e., $Eu/Eu^* \sim 1$; $Eu/Eu^* = 2Eu_N/(Sm_N + Gd_N)$ (Bau and Dulski, 1996)), and positive Y anomalies (i.e., $[Y]_N/[Ho]_N > 1$ and $Y/Y^* = 2^*[Y]_N/([Dy]_N+[Ho]_N \sim 2$) (Table S1; Fig. S6B). These REY geochemical fingerprints reflect the inherited features of a marine depositional setting (Bau et al., 1995; Zhang et al., 1994). In contrast, igneous phosphate rocks are highly enriched in light REY and depleted in heavy REY and tend to show weak negative Ce anomalies, strong positive Eu anomalies, and absence of or negative Y anomalies (e.g., phosphate rocks from South Africa and Russia; Table S1; Fig. S6B). Old-age sedimentary phosphate rocks (i.e., from China and India) show a typical enrichment of middle REY

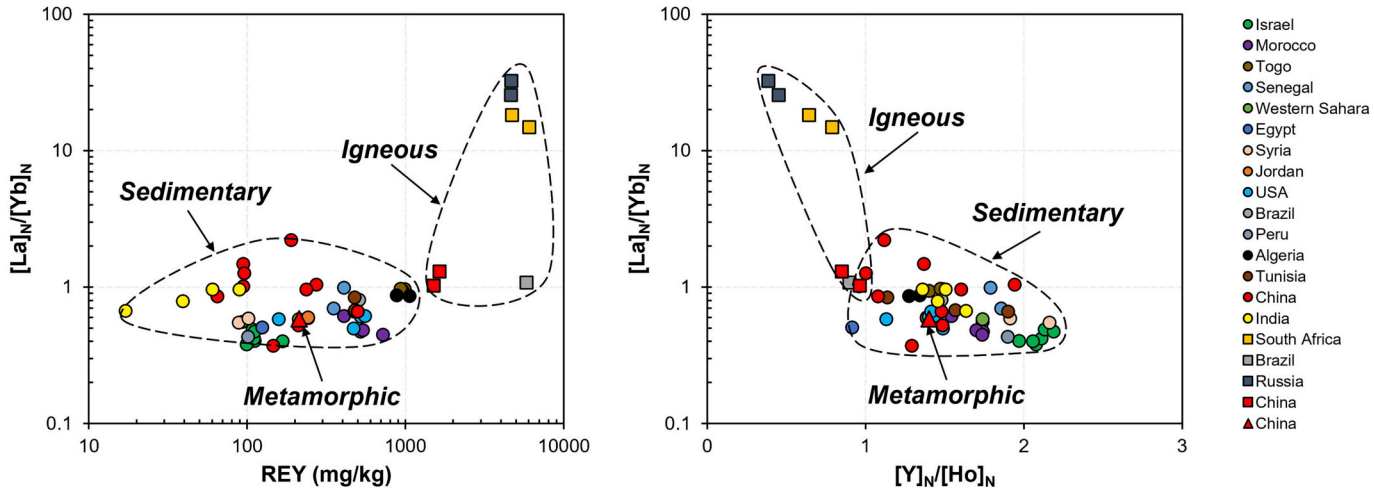

Fig. 3. Binary scatter plots of $[La]_N/[Yb]_N$ vs. REY concentration and $[Y]_N/[Ho]_N$ vs. $[La]_N/[Yb]_N$ for all phosphate rock samples analyzed in this study. Circle, square, and triangle symbolize marine sedimentary, igneous, and metamorphic types of phosphate rocks, respectively.

compared to light REY and heavy REY, with minor negative Ce and weak positive Eu anomalies (Table S1; Fig. S6B), consistent with results reported in previous studies (Emsbo et al., 2015; Jarvis, 1995; Shields and Stille, 2001; Yang et al., 2019). The REY characteristics of the analyzed Precambrian (i.e., Ediacaran) and early Cambrian sedimentary phosphate rocks from China are also consistent with previously reported values on the REY distribution in phosphate rocks of the same ages (Xin et al., 2015; Yang et al., 2022; Yang et al., 2019).

The Post-Archean Australian Shale (PAAS)-normalized REY distribution patterns of all the analyzed phosphate rock samples sorted by their geographic regions are shown in Fig. 4. Broadly, four types of REY distribution patterns can be categorized: (1) seawater-like patterns for phosphate rocks from the South Tethys (i.e., Israel, Morocco, Senegal, Western Sahara, Syria, and Jordan), as well as some of those from USA, Peru, and China (Fig. 4A-F, H), characterized by a strong negative Ce anomaly, light REY depletion, and heavy REY enrichment (Emsbo et al., 2015; Lumiste et al., 2021; McArthur and Walsh, 1984); (2) bell-shaped patterns for phosphate rocks from Egypt, Algeria, Tunisia, China, and India (Fig. 4D, G-I), with weak to little negative Ce anomaly, notable enrichment of middle REY, and depletion of both light and heavy REY (Reynard et al., 1999; Shields and Stille, 2001); (3) shale-like patterns for phosphate rocks from Togo, Brazil, and India (Fig. 4C, E-F, I), which are shown to be relatively flat and with little negative Ce anomaly and heavy REY enrichment (Lumiste et al., 2021; McArthur and Walsh, 1984); and (4) igneous patterns for the igneous phosphate rocks from South Africa, Russia, and China, with light REY enrichment and heavy REY depletion (Fig. 4J).

Notably, phosphate rock samples from China exhibit diverse REY distribution patterns. Specifically, the early Cambrian – late Devonian rocks sourced from southwestern China (i.e., Guizhou, Sichuan, and Yunnan Provinces) exhibit seawater-like patterns, whereas those of the Precambrian dominantly from Hubei Province are characterized by middle REY-enriched with a little negative Ce anomaly and even a positive Eu anomaly (Fig. 4H; Table S1). This different REY patterns between the early Cambrian and Precambrian phosphates in South China have also been documented previously (Yang et al., 2022).

4. Discussion

4.1. Overprinted Pb isotope compositions

The initial Pb isotope composition is determined by the amount of U, Th, and Pb incorporated into CFA and co-occuring minerals in the phosphate rock, which would become increasingly radiogenic through geological time provided a closed system was maintained. However, it is possible that the long-term open system interaction of phosphate with the ambient diagenetic environment can perturb the initial U-Th-Pb isotopic systems by mixing with extraneous Pb (Aubineau et al., 2022; Jahn and Cuvellier, 1994), resulting in an overprinted Pb isotope composition. Fig. 2C shows that the $^{206}Pb/^{204}Pb$ and $^{207}Pb/^{204}Pb$ ratios of all phosphate rock samples, except those from India, form the same linear array, which indicates a mixing relationship between the in-situ radiogenic Pb and extraneous Pb sources (Jahn and Cuvellier, 1994), rather than variations as a result of age difference. This can be evidenced by the Pb—Pb isochron plots (i.e., $^{207}Pb/^{204}Pb$ vs. $^{206}Pb/^{204}Pb$) as depicted in Fig. S7, where the reference isochrons of 1921 Ma, 1330 Ma, and 531 Ma were included (Chen et al., 2004; Jiang et al., 2006; Sarangi et al., 2004). Fig. S7 shows that the old-age phosphate rocks from India and China scatter notably on the Pb—Pb isochron plots and do not follow the respective references isochrons (i.e., the geological ages of the phosphate rock formations from India and China are 1921 Ma and 531 Ma, respectively). In comparison, the younger-age phosphate rocks such as those from Israel and Morocco appear to form straight regression lines, whose slopes approximately correspond to that of isochrons of ~108 Ma and ~ 151 Ma, respectively (Fig. S7), which, however, are not consistent with their geological ages of 72–83 Ma and 56–66 Ma, respectively (Table S1). Such discrepancy suggests that there is no geologically reliable and meaningful age information that can be discerned from the Pb isotope compositions of these investigated phosphate rocks (Fig. S7). Moreover, phosphate rocks primarily contain apatite phase that belongs to the *Zircon Group* with high U/Pb ratios and thus markedly high $^{206}Pb/^{204}Pb$ ratios of 500–40,000, compared to lower ratios of rocks from the *Galena Group* (< 18.7) and *Crustal Rock Group* (15–30) (Jahn and Cuvellier, 1994). The extremely high $^{206}Pb/^{204}Pb$ ratios expected in phosphate can be attributed to the selective removal of U from seawater into the porewater, which is largely incorporated into the CFA under reducing conditions (Sun et al., 2020). However, the $^{206}Pb/^{204}Pb$ ratios of the sedimentary phosphate rocks investigated in this study show lower ratios of $^{206}Pb/^{204}Pb$, ranging from 18 to 70 (Table S1), which likely indicates the incorporation of extraneous crustal Pb into and/or expulsion of U from the original U—Pb system due to diagenetic alterations (Jahn and Cuvellier, 1994).

The $^{206}Pb/^{204}Pb$ ratios of the sedimentary phosphate rocks exhibit a negative correlation with Pb concentrations ($\rho = -0.62$, $p = 3.8 \times 10^{-7}$; Fig. 5A) and a positive correlation with U/Pb ratios ($\rho = 0.75$, $p = 2.2 \times 10^{-16}$; Fig. 5B). Among all the sedimentary phosphate rocks, those from Israel and Morocco have the highest $^{206}Pb/^{204}Pb$ ratios and U/Pb ratios (Fig. 5B), suggesting the least extent of alteration compared to other

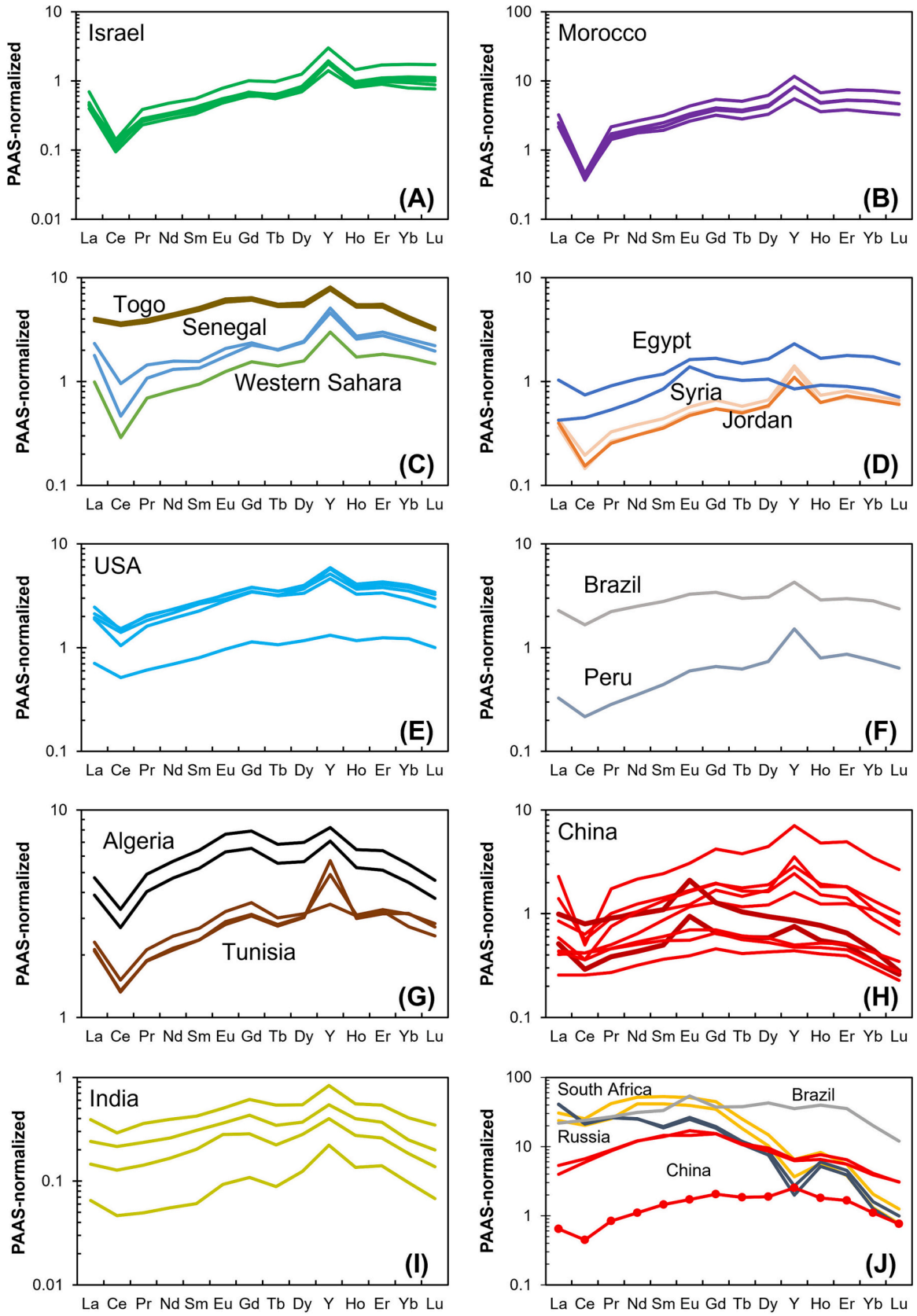

Fig. 4. The Post-Archean Australian Shale (PAAS)-normalized REY distribution patterns for all phosphate rock samples analyzed in this study. (A) – (I) depict the patterns of marine sedimentary type phosphate rocks, and (J) depicts patterns of igneous rocks and one metamorphic rock from China (red line with circle markers). Darker red in (H) highlights sedimentary samples from China with notable positive Eu anomalies. (For interpretation of the references to colour in this figure legend, the reader is referred to the web version of this article.)

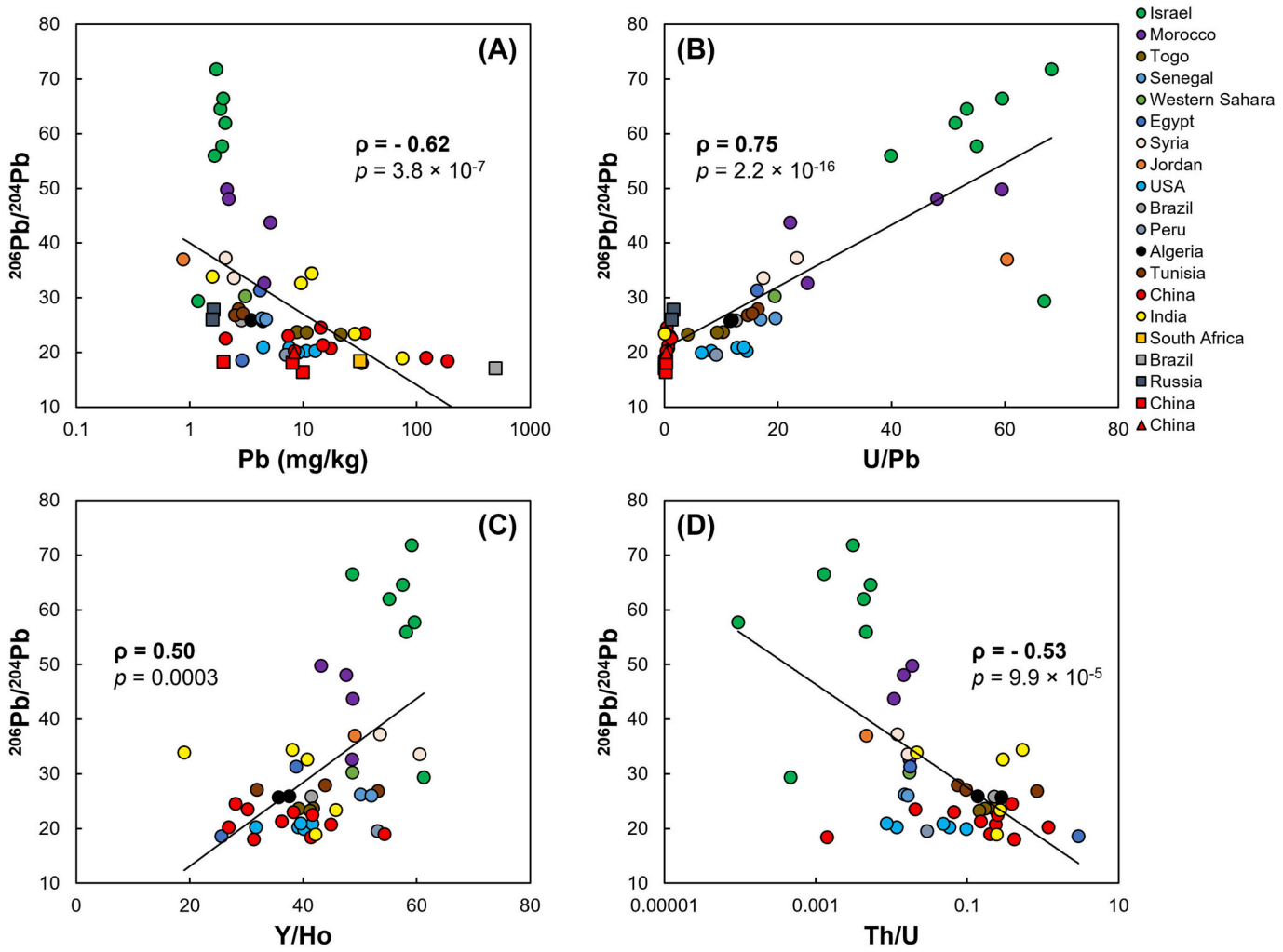

Fig. 5. Binary scatter plots of $^{206}Pb/^{204}Pb$ vs. elemental concentration and ratios for all phosphate rock samples analyzed in this study. (A) $^{206}Pb/^{204}Pb$ vs. Pb concentration. (B) $^{206}Pb/^{204}Pb$ vs. U/Pb. (C) $^{206}Pb/^{204}Pb$ vs. Y/Ho. (D) $^{206}Pb/^{204}Pb$ vs. Th/U. Circle, square, and triangle symbolize marine sedimentary, igneous, and metamorphic types of phosphate, respectively.

sedimentary phosphate rocks from the southern Tethys, the eastern U.S., China, and India. The very low U/Pb ratios in the old phosphate rocks from China and India could be derived from the interaction with terrestrial fluids during post-depositional diagenesis and/or metamorphism (Jahn and Cuvellier, 1994), which would result in the addition of extraneous Pb. Such extraneous Pb could be contributed from the landward transport to the shallow marine settings that characterized phosphate depositional environment, whereby phosphate can be physically reworked to form phosphate pellets and possibly diluted and mixed with terrestrial materials (El Bamiki et al., 2021; Pufahl and Groat, 2017). For example, the U.S. phosphate deposits were formed in a shallow-water shelf (Compton et al., 1993) in contrast to the intermediate – deep waters in the Tethys Basin (Soudry et al., 2006). The less radiogenic Pb isotope compositions in the U.S. samples might be influenced by the seawater transgression during the Mid-Miocene, which transferred phosphate landward and caused the mixing with terrestrial materials (Compton et al., 1993; Van Kauwenbergh et al., 1990). The positive correlation between Pb concentration and Al concentration in the younger sedimentary samples can further support the influences of terrestrial materials on Pb in phosphate ($\rho = 0.83$, $p = 2.5 \times 10^{-7}$; Fig. S8). Alternatively, the low U/Pb ratios in the older phosphate rocks can reflect depositional environment without the enrichment of U in CFA in the diagenetic environment due to anoxic bottom seawater during the Precambrian.

The interaction with terrestrial fluids can also be reflected by the moderate positive correlation displayed between $^{206}Pb/^{204}Pb$ and Y/Ho for all the sedimentary phosphate rocks analyzed in this study ($\rho = 0.50$, $p = 0.0003$; Fig. 5C). As the terrestrial contribution increases, the Y/Ho ratio is expected to shift away from typical seawater values (i.e., Y/Ho = 40–70; Fig. 5C) due to the chemical fractionation between Y and Ho (Zhang et al., 1994). While Y is more weakly complexed with carbonate ions than Ho during scavenging in surface water, whereas in deep seawater, Y is complexed with carbonate ions equally or stronger than Ho, which explains why Y/Ho in terrestrial source is lower than that in seawater (Bolhar et al., 2004; Zhang et al., 1994). Phosphate rocks from Israel, Morocco, Syria, and Jordan that have the most radiogenic $^{206}Pb/^{204}Pb$ ratios also have Y/Ho ratios close to the marine signature (Fig. 5C), suggesting less terrestrial input (Lumiste et al., 2021; Zhang et al., 1994). In contrast, those phosphate rocks with the least radiogenic Pb isotope ratios have the lowest Y/Ho ratios, close to that of the terrestrial fingerprint (~ 26) (Bolhar et al., 2004). Likewise, the negative correlation between $^{206}Pb/^{204}Pb$ and Th/U in the sedimentary phosphate rocks ($\rho = -0.53$, $p = 9.9 \times 10^{-5}$) suggests that terrestrial input (i.e., high Th) is an important factor for the less radiogenic Pb isotope compositions (Fig. 5D). The imprints of low Y/Ho and high Th/U ratios in the phosphate rocks reflect a higher extent of mixing with terrestrial matrials. Furthermore, the detection of accessory minerals like quartz and albite in some of the phosphate rock samples can also provide

evidence for the contribution of terrestrial materials (Figs. S6–8). In contrast, the phosphate rocks from Israel and Morocco have a rare occurrence of these accessory minerals (Fig. S6). Although the intra-basin variations of Pb isotope compositions can be largely explained by their different contributions of terrestrial sources, the observed variations within the same region of origin (e.g., China) may suggest their differences in the initial U and Th geochemistry and/or the influences of other factors such as depositional conditions and diagenetic effects (see discussion in Section 4.3.).

4.2. Altered REY seawater signatures

The REY composition of seawater is characterized by strong negative Ce anomalies (Bolhar et al., 2004; Shields and Webb, 2004; Zhang et al., 1994). Authigenic phosphate deposits tends to inherit such characteristic negative Ce anomalies when REY are incorporated into CFA under the equilibrium with pore water originating from bottom seawater (Auer et al., 2017; Picard et al., 2002). However, the Ce/Ce* values can be influenced by the anomalies of La due to either surface weathering or diagenesis (McArthur and Walsh, 1984), which then could lead to false Ce anomalies. To counteract this effect and discern the true Ce anomalies, Pr/Pr* (Pr/Pr* = $2[Pr]_N/([Ce]_N+[Nd]_N)$ was proposed to pair with Ce/Ce* (Bau and Dulski, 1996). Fig. 6A shows that most of the phosphate rocks fall within Field IIIb, suggesting that their negative Ce anomalies are authentic, whereas certain phosphate rocks, including those from China and India, have only minor negative Ce anomalies and plot within Field IIa. This suggests that their Ce/Ce* values may have been exaggerated by positive La anomalies (Bau and Dulski, 1996), and they should instead have little negative Ce anomalies or even minor positive Ce anomalies.

Another typical REY feature of seawater is the depletion of light REY relative to heavy REY (Bolhar et al., 2004; McArthur and Walsh, 1984). The pairs of Ce/Ce* with $[Dy]_N/[Yb]_N$ and $[Pr]_N/[Yb]_N$, respectively can be used to show the deviation of phosphate REY compositions from seawater signature. The $[Dy]_N/[Yb]_N$ ratios of most phosphate rocks are around 0.8–1.1 (Fig. 6C), indicative of a similar composition to modern seawater, except those from China, India, and the igneous type. Similarly, as shown in Fig. 6D, an obvious light REY enrichment (i.e., $[Pr]_N/[Yb]_N > 1$) is observed in the phosphate rocks from China, India, and those of igneous type. Among all the analyzed phosphate rocks, those from Israel and Morocco appear to have the best preserved seawater REY signatures, while the rest of samples exhibit altered seawater signatures to varying extent (Fig. 4 and Fig. 6). The preserved seawater REY signature coincides with the more radiogenic Pb isotope composition of the phosphate rocks from Israel and Morocco.

A common non-seawater REY signature in phosphate rocks is the enrichment of middle REY (i.e., bell-shaped distribution pattern), as shown in the phosphate rocks from Algeria, Tunisia, and China (Fig. 4G-H). The ratio of $[Dy]_N/[Sm]_N$ has been used as an indicator of the effect of middle REY enrichment (Shields and Stille, 2001), which is largely invariable in seawater ($[Dy]_N/[Sm]_N \sim 2$) and decreases as a result of incorporation of middle REY. The preferential uptake of middle REY (i.e., $[Dy]_N/[Sm]_N < 2$) has been suggested to take place due to prolonged exposure to seawater during decomposition and physical reworking of marine sedimentary phosphates (Auer et al., 2017; Reynard et al., 1999), and/or is reflective of the effects of diagenetic modification (German and Elderfield, 1990; Shields and Stille, 2001). The binary plot of $[Dy]_N/[Sm]_N$ vs. Ce/Ce* for all the analyzed phosphate rocks shows a

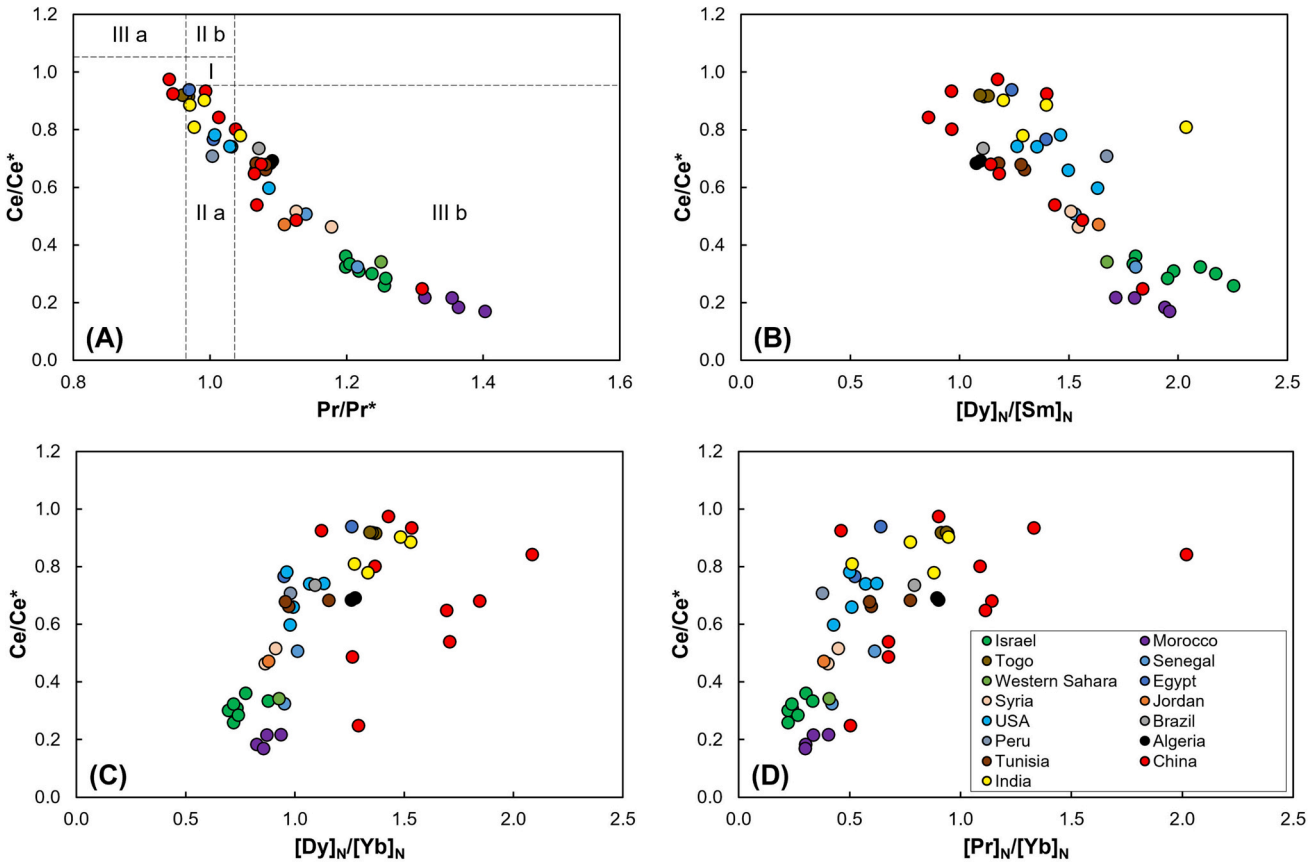

Fig. 6. Binary scatter plots of Ce/Ce* vs. other REY indices for all marine sedimentary phosphate rock samples analyzed in this study. (A) Ce/Ce* vs. Pr/Pr* after (Bau and Dulski, 1996). Field I: no Ce anomaly; Field IIa: negative Ce anomaly caused by positive La anomaly; Field IIb: positive Ce anomaly caused by negative La anomaly; Field IIIa: authentic positive Ce anomaly; Field IIIb: authentic negative Ce anomaly. (B) Ce/Ce* vs. $[Dy]_N/[Sm]_N$. (C) Ce/Ce* vs. $[Dy]_N/[Yb]_N$. (D) Ce/Ce* vs. $[Pr]_N/[Yb]_N$.

negative correlation (Fig. 6B), suggesting that the chemical compositions of those phosphate rocks with low $[Dy]_N/[Sm]_N$ and high Ce/Ce* values may have been altered after deposition with progressive scavenging of middle REY from seawater and then into porewater, implying their open-system behavior that may cause the input of REY from terrigenous materials such as detrital siliciclastic sediments (Xin et al., 2015). Overall, the correlations observed for the different REY proxies (Fig. 5) indicate a mixing nature of phosphate rocks with the geochemical fingerprints of both the original marine depositional environment and secondary and/or diagenetic effects.

4.3. Imprints of depositional conditions and diagenetic influences

The Ce anomaly has been used for reflecting the paleoredox conditions during the depositional history of phosphates (Auer et al., 2017; German and Elderfield, 1990; Reynard et al., 1999; Shields and Stille, 2001; Yang et al., 2022). A pronounced negative Ce anomaly is often indicative of oxic conditions of seawater (Bau and Dulski, 1996; Garnit et al., 2012). Among the young-age sedimentary phosphate rocks, Fig. 6 shows that Israeli and Moroccan samples have strong negative Ce anomalies, indicating that the initial oxic condition of seawater may well be preserved in these rocks. In contrast, the other phosphate rocks have higher Ce/Ce* values, likely reflecting the impact of later diagentic alteration that led to change of seawater redox signal in them. For example, previous works have suggested the siliciclastic detrital inputs for those from Egypt, Togo, Algeria, and Tunisia when the phosphates were reworked and redeposited (Abou El-Anwar et al., 2017; Baioumy and Farouk, 2022; El Bamiki et al., 2021; Ounis et al., 2008; Soudry et al., 2006). This can be reflected by their relatively higher Ce/Ce* and lower $[Dy]_N/[Sm]_N$ values than those of phosphate rocks from Israel and Morocco (Table S1; Fig. 6B). In comparison, the Proterozoic phosphate rocks from China and India show even weaker Ce anomalies compared to the younger phosphate rocks (Table S1; Fig. 6A), which would reflect the original suboxic condition of bottom seawater. This can serve as a possible mechanism to explain the low abundance of U content reported in these old phosphate rocks (Sun et al., 2020). The Proterozoic Ocean was suggested to be stratified by shallow oxic seawater overlying deep anoxic seawater, thus resulting in suboxic seafloor pore water (Cui et al., 2016). Such conditions would result in higher Ce/Ce* values even in authigenic phosphate in equailibrium with pore water originating from suboxic bottom seawater. In contrast, the lower Ce/Ce* values observed in the early Cambrian phosphate rocks from China may reflect the change of seawater redox conditions near the Precambrian-Cambrian boundary and the transition from suboxic to oxic bottom seawater (Kimura and Watanabe, 2001; Yang et al., 2022; Yang et al., 2019).

A negative correlation between $^{206}Pb/^{204}Pb$ ratios and Ce/Ce* is observed for all the investigated sedimentary phosphate rocks in this study ($\rho = -0.50$, $p = 0.0002$; Fig. 7A). This suggests that younger phosphate rocks preserving the original oxic seawater signal (i.e., low Ce/Ce*) remain largely radiogenic (e.g., Israel and Morocco), whereas those with modifications of the initial seawater oxic condition (i.e., high Ce/Ce*) are notably influenced by detrial Pb on their isotope compositions (Fig. 7A). In comparison, the Precambrian phosphate rocks presumably deposited under suboxic seawater conditions have greater isotopic imprints of detrital Pb (Fig. 7). One possible source for such detrital Pb could be associated with the reductive dissolution of Fe oxides/oxyhydroxides in marine sediments under anoxic conditions (Basak et al., 2011), whereby adsorbed Pb particles from continental weathering was likely incorporated into phosphate during later diagenesis, leading to lower U/Pb ratios and thus lower $^{206}Pb/^{204}Pb$ ratios. It has also been suggested that the Fe redox cycling could release REY during anoxic conditions with the liberation of Ce and middle REY into pore water (Auer et al., 2017; Gong et al., 2021; McArthur and Walsh, 1984; Shields and Stille, 2001), thus causing the enrichment of middle REY and minor negative and/or weak positive Ce anomalies in phosphate rocks. Therefore, this could explain the negative correlation between the $^{206}Pb/^{204}Pb$ ratios and Ce/Ce* values (Fig. 7A) and the positive correlation exhibited between the $^{206}Pb/^{204}Pb$ ratios and $[Dy]_N/[Sm]_N$ values ($\rho = 0.48$, $p = 0.0005$; Fig. 7B).

Emsbo et al. (2015) have suggested that the differences in REY patterns in marine sedimentary phosphate rocks of different ages reflect the secular variation of REY geochemistry in seawater. However, it has been shown that the seawater REY patterns have hardly changed throughout the Phanerozoic (Shields and Webb, 2004), which implies that post-depositional diagenetic alterations and/or in-situ water-rock interactions would be the major cause for the deviations of REY patterns of phosphate rocks from that of modern seawater (Elderfield and Pagett, 1986; Picard et al., 2002; Wright et al., 1987). The $[La]_N/[Sm]_N$ and $[La]_N/[Yb]_N$ ratios have been used to delineate the impact of diagenetic alteration (Reynard et al., 1999). The binary plot of $[La]_N/[Yb]_N$ vs. $[La]_N/[Sm]_N$ (Fig. 8) shows that the REY compositions of most phosphate rocks deviate from that of modern seawater of 0.2–0.5 for $[La]_N/[Yb]_N$ and 0.6–1.6 for $[La]_N/[Sm]_N$ (Reynard et al., 1999), particularly for the phosphate rocks from China, India, Algeria, Tunisia, and Senegal. The variations of $[La]_N/[Yb]_N$ and $[La]_N/[Sm]_N$ are plotted above the seawater compositional field, indicating pronounced influences of diagenetic modification (Fig. 8). Two rock samples from China and one from Egypt exhibit somewhat effects of substitution, whereas those from

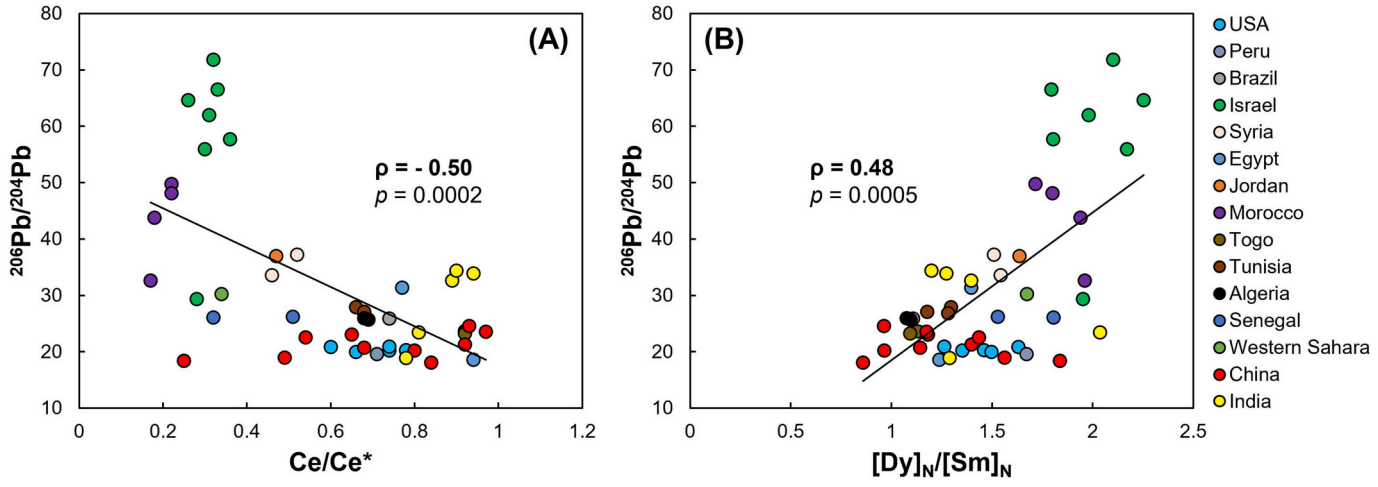

Fig. 7. Binary scatter plots of $^{206}Pb/^{204}Pb$ vs. REY indices for all marine sedimentary type phosphate rock samples analyzed in this study. (A) $^{206}Pb/^{204}Pb$ vs. Ce/Ce*. (B) $^{206}Pb/^{204}Pb$ vs. $[Dy]_N/[Sm]_N$.

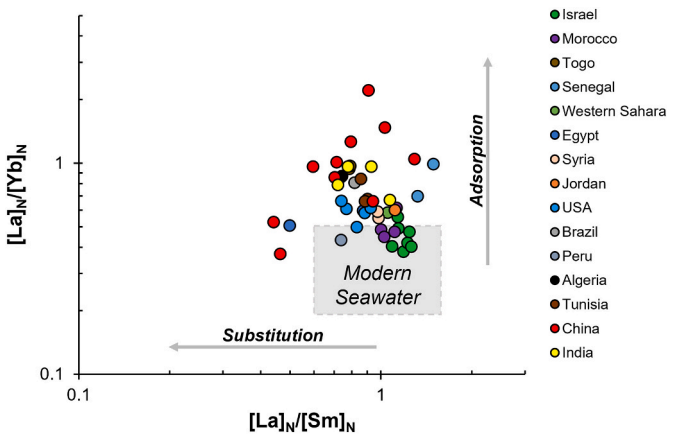

Fig. 8. Binary scatter plot of $[La]_N/[Yb]_N$ vs. $[La]_N/[Sm]_N$ proposed by (Reynard et al., 1999) for all marine sedimentary type phosphate rock samples analyzed in this study.

Israel, Morocco, and Peru are plotted within the seawater compositional field (Fig. 8), indicating little diagenetic alteration. The rest of phosphate rocks show minor to moderate diagenetic effects (e.g., those from the U.S.; Fig. 8). In addition, it has been suggested that diagenesis can decrease the La content and increase the Y anomaly (Shields and Stille, 2001). As shown in Fig. S9, Y/Y* displays a positive correlation with $[La]_N/[Nd]_N$ for all the marine sedimentary phosphate rocks, indicating the effect of diagenesis on most of the rocks except those from Israel and Morocco, whereas there does not appear to be any weathering effects. Consistently, phosphate rocks from China, India, and the U.S. contain carbonate minerals (i.e., dolomite) and quartz (Figs. S7–8), likely resulting from the interaction with diagenetic fluids (Cui et al., 2016; Van Kauwenbergh et al., 1990). The diagnenetic alteration could also be reflected by the coincident low U concentrations and low $\delta^{18}O$ ratios in the Chinese phosphate rocks, which may indicate the influence of meteoric waters (Sun et al., 2020). Overall, phosphate rocks with the least effects of diagenetic alteration as indicated by the seawater REY characteristics coincide with the most radiogenic Pb isotope compositions, such as those from Israel and Morocco.

4.4. Implications for environmental tracing

Given that the environmental impacts of phosphate mining and P-fertilizer production and application are commonly associated with elevated concentrations of trace metals (e.g., U and Cd) and activities of radionuclides (e.g., ^{238}U and ^{226}Ra) (Aoun et al., 2010; El-Bahi et al., 2017; Fayiga and Nwoke, 2016; Gaudry et al., 2007; Makweba and Holm, 1993; Martínez-Aguirre et al., 1994; Pérez-López et al., 2010; Rutherford et al., 1995; Rutherford et al., 1994; Schnug et al., 2023; Vengosh et al., 2022), we suggest that use of Pb isotopes could help to constrain the origin and influence of phosphate-derived contamination relative to other natural and anthropogenic sources and their impacts on the environment (Abi-Ghanem et al., 2009; Gaudry et al., 2007; Kamenov et al., 2009; Roy and Négrel, 2001). The Pb isotope compositions of all the analyzed phosphate rocks define a global Pb array on the $^{208}Pb/^{206}Pb$ vs. $^{206}Pb/^{207}Pb$ plot, except for the igneous phosphate rocks from Russia (Fig. 9A). This phosphate Pb array is distinct from the array of global Pb ore deposits defined by representative ore deposits around the world (i.e., Broken Hill, Australia; Beddiane, Morocco; San Vicente, Peru; and Mississippi Valley Type, USA; Fig. 9) (Sangster et al., 2000). Most of the sedimentary phosphate rocks have a more radiogenic Pb composition than the Pb ore deposits, which are the major sources for Pb additives (i.e., alkyl-lead) used in gasoline, representing one of the important legacy anthropogenic Pb sources in the environment (Bi et al., 2017; Bollhöfer and Rosman, 2002; Bollhöfer and Rosman, 2001; Komárek et al., 2008). For example, the Broken Hill ore deposits from Australia and the Mississippi Valley Type (MVT) ore deposits from the U. S. are two of the major sources for alkyl-lead (Bollhöfer and Rosman, 2002; Bollhöfer and Rosman, 2001), and their different isotope compositions reflect the Pb isotopic signatures of leaded gasoline in Europe and North America, respectively (Komárek et al., 2008). In addition, the Pb isotope compositions of pesticides and herbicides (Ayuso et al., 2004) are shown to largely follow along the array of Pb ore deposits that notably deviates from that of phosphate Pb as well as the natural crustal Pb (Komárek et al., 2008) (Fig. 9B). The distinctive radiogenic Pb isotope composition of phosphate rocks, except some of those of igneous type from China, South Africa, and Brazil (Fig. 9B), compared to that of the other major anthropogenic (i.e., Pb ore deposits and pesticides and herbicides) and natural crustal Pb sources is potentially advantageous for using Pb isotopes to trace contaminants in the environment derived from phosphate rock (e.g., wastewater derived from phosphate

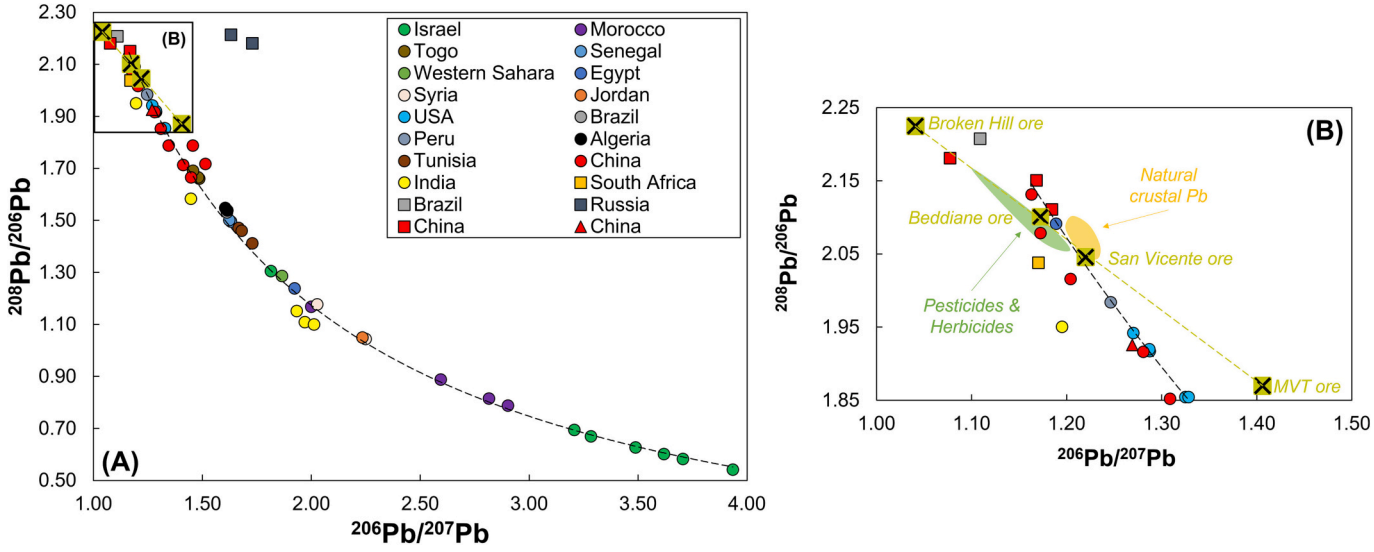

Fig. 9. Binary scatter plots of $^{208}Pb/^{206}Pb$ vs. $^{206}Pb/^{207}Pb$ ratios for all phosphate rock samples analyzed in this study. Circle, square, and triangle symbolize marine sedimentary, igneous, and metamorphic types of phosphate, respectively. Data on Pb ore deposits are from Sangster et al. (2000). Data on pesticides and herbicides are from Ayuso et al. (2004). Data on natural crustal Pb are from Komárek et al. (2008).

mining)), phosphate fertilizer used in agriculture, and phosphogypsum, which is the byproduct of ferilizers production from phosphate rocks.

The $^{208}Pb/^{206}Pb$, $^{206}Pb/^{207}Pb$, $^{206}Pb/^{204}Pb$, and Ce/Ce* ratios of P-fertilizer samples from the U.S. (n = 4), China (n = 4), Israel (n = 3), Morocco (n = 1), Jordan (n = 1), and India (n = 1) are presented in Table S2. Consistent with the Pb isotope composition of the phosphate rocks, the P-fertilizers from Israel are characterized by highly radiogenic Pb isotope ratios, whereas those from the U.S., China, and India have much less radiogenic Pb isotope composition (Fig. 10A). Although the Pb isotope compositions of most analyzed P-fertilizer samples are within the range of respective phosphate rocks of the same region, they can have large variations and deviation from that of phosphate rocks, as reflected by samples from the U.S. and Morocco (Fig. 10A). This might be due to the possibility that these phosphate rocks and fertilizers are not exactly from the same manufacturer, and/or the production of fertilizer is not always subject to the use of a single source of phosphate rock. It should also be acknowledged that the Pb isotope variations in each phosphate deposit may well be larger than the isotope range reported in this study. Yet, all the P-fertilizer samples analyzed in this study fall on the same Pb array defined by the isotope compositions of phosphate rocks (Fig. 10A), which is distinct from that of Pb ore deposits, pesticides/herbicides, and natural crustal Pb (Fig. 9). This reinforces the advantage of using Pb isotopes as a tracer for disentangling the sources of contaminants from phosphate fertilizers and waste products relative to other natural and anthropogenic sources. This also implies that there is minimal additional Pb being introduced during the P-fertilizer production, and that Pb in P-fertilizer primarily inherits the isotopic signature of the parent phosphate rocks. The binary plot of $^{206}Pb/^{204}Pb$ vs. Ce/Ce* (Fig. 10B) further shows that the P-fertilizer samples from China, Israel, Jordan, and India largely fall within the compositional field defined by the respective phosphate rocks, indicating similar geochemical compositions. In contrast, the geochemical signatures of the P-fertilizer samples from the U.S. and Morocco obviously deviate from the corresponding phosphate rocks (Fig. 10B). The type of the Moroccan fertilizer is phosphate-potassium fertilizer (Table S2), which may implicate that additional source of Pb and REY has been introduced with the addition of the K source. Overall, our results show that, in cases of the single-source phosphate rock being used for fertilizer production, both the Pb isotopes and REY characteristics may well be preserved in the phosphate fertilizers and are consistent with the original phosphate rocks, indicating the potential utility of combination of Pb isotopes and REY as an environmental tracer for soils and waters impacted by phosphate fertilizer production and application.

5. Conclusions

This study presents the Pb isotope and REY compositions of phosphate rocks sourced from different geographic regions in the world, covering major economic phosphate deposits, including those from China, Southern Tethys (e.g., Morocco, Tunisia, Israel), eastern U.S., South Africa, and Russia. The Pb isotope compositions of phosphate rocks of different sources and geological ages show large variations. Generally, phosphate rocks of marine sedimentary type have more radiogenic Pb isotope compositions than those of igneous type, of which igneous phosphate rocks from Russia are distinctively different from those of other regions. Among the sedimentary rocks, the Pb isotope compositions of phosphate rocks from the Southern Tethys are significantly more radiogenic than that of phosphate rocks from China and the eastern U.S. Within the Southern Tethyan region, phosphate rocks from Israel are the most radiogenic in Pb, followed by those from Morocco, Syria, Jordan, Egypt, Western Sahara, Tunisia, Senegal, Algeria, and Togo.

The results of this study show that the radiogenic Pb isotope composition of the phosphate rocks have been overprinted by non-radiogenic terrestrial Pb, although the mineralogical data reveal that most of these rocks are dominantly composed of carbonate fluorapatite (francolite), with low aboundance of other minerals in the young (i.e., Late Cretatous to Mid-Miocene) phosphate rocks. The extent of such overprinting effect is observed the least in the Israeli and Moroccan phosphate rocks compared to the rest of sedimentary phosphate rocks. The variations of Pb isotope compositions of phosphate rocks are likely influenced jointly by their original U/Pb and Th/Pb ratios, as well as differences in the depositional conditions and/or diagenetic modifications, which can be largely reflected also by their REY characteristics. Specifically, marine sedimentary phosphate rocks that inherited relatively pristine seawater REY distribution feature likely reflect the preservation of oxic bottom seawater condition and/or with minimal diagenetic alteration, resulting in a more radiogenic Pb isotope composition, such as those from Israel and Morocco. In contrast, phosphate rocks with REY indications for more anoxic bottom seawater and/or greater diagenetic alteration could lead to the deviation from the seawater REY signatures, coninciding with less radiogenic Pb isotope compositions that indicate the mixing with non-radiogenic terrestrial Pb.

This study further evaluates the potential utility of Pb isotopes and their combination with REY proxies for tracing the contamination of phosphate mining and P-fertilizer production and application in the environment. The distinctively radiogenic Pb isotope composition of most of the phosphate rocks compared to those of both natural crustal Pb and major anthropogenic Pb sources (e.g., Pb ore deposits and

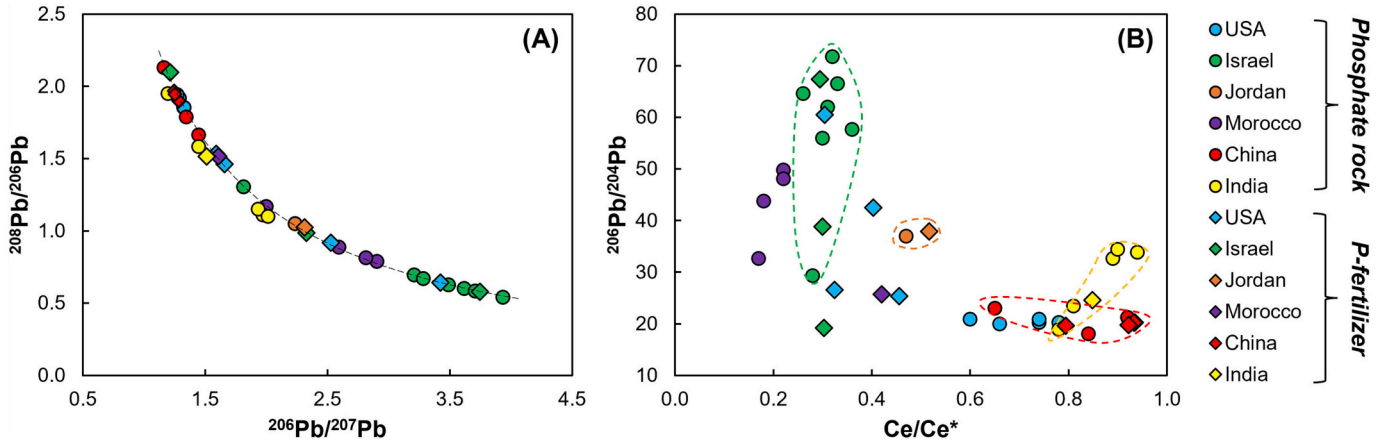

Fig. 10. Binary scatter plots of (A) $^{208}Pb/^{206}Pb$ vs. $^{206}Pb/^{207}Pb$ and (B) $^{206}Pb/^{204}Pb$ vs. Ce/Ce* for phosphate rock and P-fertilizer samples sourced from the same regions of origin.

pesticides) provides a novel approach for detecting metal(loid) contamination in the environment from phosphate sources. Although the Pb isotope compositions of P-fertilizer samples can show large variations from that of phosphate rocks of the same source region, their Pb isotope variations are largely within the composition defined by the phosphate rocks, bearing the same isotopic distinction from the other Pb sources. The combination of Pb isotope ratios and REY proxies could further constrain the source discrimination. Overall, this study provides a dataset for Pb isotopes and rare earth elements in global phosphate rocks, which lays the groundwork for future regional and local studies on both their geological and environmental implications.

Declaration of Competing Interest

The authors declare that they have no known competing financial interests or personal relationships that could have appeared to influence the work reported in this paper.

Data availability

All data are presented in the paper

Acknowledgements

We sincerely appreciate M. Abu-Hashim, O. Duckworth, L. Gatiboni, T. El-Hasan, S. Haneklaus, A. Singh, A. Shrivastava, and P. Zhang for their collegiality in sharing phosphate rock and fertilizer samples with us. We thank for the access to XRD at the Duke University Shared Materials Instrumentation Facility (SMIF), a member of the North Carolina Research Triangle Nanotechnology Network (RTNN), which is supported by the National Science Foundation (award number ECCS-2025064) as part of the National Nanotechnology Coordinated infrastructure (NNCI). This study was conducted in preparation for NSF funded project "*From Global to Local: Geochemistry of Global Phosphate Ores and Implications for Tracing the Environmental Impacts of Fertilizers Utilization*" (EAR- 2305946). We thank the two annonomous reviewers for their critical comments that have greatly improved the quality of this manuscript.

Appendix A. Supplementary data

Supplementary data to this article can be found online at https://doi.org/10.1016/j.chemgeo.2023.121715.

References

Abi-Ghanem, C., Chiffoleau, J.F., Bermond, A., Nakhlé, K., Khalaf, G., Borschneck, D., Cossa, D., 2009. Lead and its isotopes in the sediment of three sites on the Lebanese coast: Identification of contamination sources and mobility. Appl. Geochem. 24, 1990–1999. https://doi.org/10.1016/j.apgeochem.2009.07.012.

Abou El-Anwar, E.A., Mekky, H.S., Abd El Rahim, S.H., Aita, S.K., 2017. Mineralogical, geochemical characteristics and origin of late cretaceous phosphorite in Duwi Formation (Geble Duwi Mine), Red Sea region, Egypt. Egypt. J. Pet. 26, 157–169. https://doi.org/10.1016/j.ejpe.2016.01.004.

Abouzeid, A.-Z.M., El-Jallad, I.S., 1980. On leaching lime and calcite from calcined calcareous phosphate with triammonium citrate solution. Int. J. Miner. Process. 7, 147–150. https://doi.org/10.1016/0301-7516(80)90006-X.

Aoun, M., El Samrani, A.G., Lartiges, B.S., Kazpard, V., Saad, Z., 2010. Releases of phosphate fertilizer industry in the surrounding environment: Investigation on heavy metals and polonium-210 in soil. J. Environ. Sci. 22, 1387–1397. https://doi.org/10.1016/S1001-0742(09)60247-3.

Aubineau, J., Parat, F., Chi Fru, E., El Bamiki, R., Mauguin, O., Baron, F., Poujol, M., Séranne, M., 2022. Geodynamic seawater-sediment porewater evolution of the east Central Atlantic Paleogene Ocean margin revealed by U-Pb dating of sedimentary phosphates. Front. Earth Sci. 10.

Auer, G., Reuter, M., Hauzenberger, C.A., Piller, W.E., 2017. The impact of transport processes on rare earth element patterns in marine authigenic and biogenic phosphates. Geochim. Cosmochim. Acta 203, 140–156. https://doi.org/10.1016/j.gca.2017.01.001.

Ayuso, R.A., Foley, N.K., Robinson, G., Wandless, G., Dillingham, J., 2004. Lead Isotopic Compositions of Common Arsenical Pesticides Used in New England (No. USGS Open-File Report 2004-1342).

Baioumy, H., Farouk, S., 2022. The geochemical and economic significance of REE in the Upper Cretaceous-Eocene Tethyan phosphorites. J. Afr. Earth Sci. 194, 104635 https://doi.org/10.1016/j.jafrearsci.2022.104635.

Basak, C., Martin, E.E., Kamenov, G.D., 2011. Seawater Pb isotopes extracted from Cenozoic marine sediments. Chem. Geol. 286, 94–108. https://doi.org/10.1016/j.chemgeo.2011.04.007.

Bau, M., Dulski, P., 1996. Distribution of yttrium and rare-earth elements in the Penge and Kuruman iron-formations, Transvaal Supergroup, South Africa. Precamb. Res., Geol. Geochem. Transvaal Supergroup 79, 37–55. https://doi.org/10.1016/0301-9268(95)00087-9.

Bau, M., Dulski, P., Moller, P., 1995. Yttrium and holmium in South Pacific seawater: vertical distribution and possible fractionation mechanisms. Chem. Erde-Geochem. 55, 1–15.

Bi, X.-Y., Li, Z.-G., Wang, S.-X., Zhang, L., Xu, R., Liu, J.-L., Yang, H.-M., Guo, M.-Z., 2017. Lead Isotopic Compositions of selected Coals, Pb/Zn Ores and Fuels in China and the Application for Source Tracing. Environ. Sci. Technol. 51, 13502–13508. https://doi.org/10.1021/acs.est.7b04119.

Bolhar, R., Kamber, B.S., Moorbath, S., Fedo, C.M., Whitehouse, M.J., 2004. Characterisation of early Archaean chemical sediments by trace element signatures. Earth Planet. Sci. Lett. 222, 43–60. https://doi.org/10.1016/j.epsl.2004.02.016.

Bollhöfer, A., Rosman, K.J.R., 2001. Isotopic source signatures for atmospheric lead: the Northern Hemisphere. Geochim. Cosmochim. Acta 65, 1727–1740. https://doi.org/10.1016/S0016-7037(00)00630-X.

Bollhöfer, A., Rosman, K.J.R., 2002. The temporal stability in lead isotopic signatures at selected sites in the Southern and Northern Hemispheres. Geochim. Cosmochim. Acta 66, 1375–1386. https://doi.org/10.1016/S0016-7037(01)00862-6.

Chen, D.F., Dong, W.Q., Zhu, B.Q., Chen, X.P., 2004. Pb–Pb ages of Neoproterozoic Doushantuo phosphorites in South China: constraints on early metazoan evolution and glaciation events. Precambrian Res. 132, 123–132. https://doi.org/10.1016/j.precamres.2004.02.005.

Compton, J.S., Hodell, D.A., Garrido, J.R., Mallinson, D.J., 1993. Origin and age of phosphorite from the south-Central Florida Platform: Relation of phosphogenesis to sea-level fluctuations and δ13C excursions. Geochim. Cosmochim. Acta 57, 131–146. https://doi.org/10.1016/0016-7037(93)90474-B.

Cook, P.J., Shergold, J.H., 2005. Phosphate Deposits of the World: Volume 1, Proterozoic and Cambrian Phosphorites. Cambridge University Press.

Cui, H., Xiao, S., Zhou, C., Peng, Y., Kaufman, A.J., Plummer, R.E., 2016. Phosphogenesis associated with the Shuram Excursion: Petrographic and geochemical observations from the Ediacaran Doushantuo Formation of South China. Sediment. Geol. 341, 134–146. https://doi.org/10.1016/j.sedgeo.2016.05.008.

El Bamiki, R., Raji, O., Ouabid, M., Elghali, A., Khadiri Yazami, O., Bodinier, J.-L., 2021. Phosphate Rocks: a Review of Sedimentary and Igneous Occurrences in Morocco. Minerals 11, 1137. https://doi.org/10.3390/min11101137.

El-Bahi, S.M., Sroor, A., Mohamed, G.Y., El-Gendy, N.S., 2017. Radiological impact of natural radioactivity in Egyptian phosphate rocks, phosphogypsum and phosphate fertilizers. Appl. Radiat. Isot. 123, 121–127. https://doi.org/10.1016/j.apradiso.2017.02.031.

Elderfield, H., Pagett, R., 1986. Rare earth elements in ichthyoliths: Variations with redox conditions and depositional environment. science of the total environment. Analyt. Chem. Marine Sci. 49, 175–197. https://doi.org/10.1016/0048-9697(86)90239-1.

Emsbo, P., McLaughlin, P.I., Breit, G.N., du Bray, E.A., Koenig, A.E., 2015. Rare earth elements in sedimentary phosphate deposits: solution to the global REE crisis? Gondwana Res. 27, 776–785. https://doi.org/10.1016/j.gr.2014.10.008.

Emsbo, P., McLaughlin, P.I., du Bray, E.A., Anderson, E.D., Vandenbroucke, T.R.A., Zielinski, R.A., 2016. Rare earth elements in sedimentary phosphorite deposits: a global assessment. In: Verplanck, P.L., Hitzman, M.W. (Eds.), Rare Earth and Critical Elements in Ore Deposits. Society of Economic Geologists, p. 0. https://doi.org/10.5382/Rev.18.05.

Fayiga, A.O., Nwoke, O.C., 2016. Phosphate rock: origin, importance, environmental impacts, and future roles. Environ. Rev. 24, 403–415. https://doi.org/10.1139/er-2016-0003.

Filippelli, G.M., 2011. Phosphate rock formation and marine phosphorus geochemistry: the deep time perspective. Chemosph. Phosphor. Cycle 84, 759–766. https://doi.org/10.1016/j.chemosphere.2011.02.019.

Garnit, H., Bouhlel, S., Barca, D., Chtara, C., 2012. Application of LA-ICP-MS to sedimentary phosphatic particles from Tunisian phosphorite deposits: Insights from trace elements and REE into paleo-depositional environments. Geochemistry 72, 127–139. https://doi.org/10.1016/j.chemer.2012.02.001.

Gaudry, A., Zeroual, S., Gaie-Levrel, F., Moskura, M., Boujrhal, F.-Z., El Moursli, R.C., Guessous, A., Mouradi, A., Givernaud, T., Delmas, R., 2007. Heavy Metals Pollution of the Atlantic Marine Environment by the Moroccan Phosphate Industry, as Observed through their Bioaccumulation in Ulva Lactuca. Water Air Soil Pollut. 178, 267–285. https://doi.org/10.1007/s11270-006-9196-9.

German, C.R., Elderfield, H., 1990. Application of the Ce anomaly as a paleoredox indicator: the ground rules. Paleoceanography 5, 823–833. https://doi.org/10.1029/PA005i005p00823.

Gnandi, K., Tobschall, H.J., 1999. The pollution of marine sediments by trace elements in the coastal region of Togo caused by dumping of cadmium-rich phosphorite tailing into the sea. Environ. Geol. 38, 13–24. https://doi.org/10.1007/s002540050396.

Gong, Q., Li, F., Lu, C., Wang, H., Tang, H., 2021. Tracing seawater- and terrestrial-sourced REE signatures in detritally contaminated, diagenetically altered carbonate rocks. Chem. Geol. 570, 120169 https://doi.org/10.1016/j.chemgeo.2021.120169.

Jahn, B., Cuvellier, H., 1994. Pb-Pb and U-Pb geochronology of carbonate rocks: an assessment. Chem. Geol. 115, 125–151. https://doi.org/10.1016/0009-2541(94)90149-X.

Jarvis, I., 1995. Phosphorite geochemistry: State-of-the-art and environmental concerns. Oceanogr. Lit. Rev. 8, 639.
Jiang, S.-Y., Chen, Y.-Q., Ling, H.-F., Yang, J.-H., Feng, H.-Z., Ni, P., 2006. Trace- and rare-earth element geochemistry and Pb–Pb dating of black shales and intercalated Ni–Mo–PGE–Au sulfide ores in lower Cambrian strata, Yangtze Platform, South China. Mineral. Deposita 41, 453–467. https://doi.org/10.1007/s00126-006-0066-6.
Kamenov, G.D., Brenner, M., Tucker, J.L., 2009. Anthropogenic versus natural control on trace element and Sr–Nd–Pb isotope stratigraphy in peat sediments of Southeast Florida (USA), ~1500 AD to present. Geochim. Cosmochim. Acta 73, 3549–3567. https://doi.org/10.1016/j.gca.2009.03.017.
Kimura, H., Watanabe, Y., 2001. Oceanic anoxia at the Precambrian-Cambrian boundary. Geology 29, 995–998. https://doi.org/10.1130/0091-7613(2001)029<0995:OAATPC>2.0.CO;2.
Komárek, M., Ettler, V., Chrastný, V., Mihaljevič, M., 2008. Lead isotopes in environmental sciences: a review. Environ. Int. 34, 562–577. https://doi.org/10.1016/j.envint.2007.10.005.
Lumiste, K., Lang, L., Paiste, P., Lepland, A., Kirsimäe, K., 2021. Heterogeneous REE + Y distribution in early Paleozoic shelly phosphorites: Implications for enrichment mechanisms. Chem. Geol. 586, 120590 https://doi.org/10.1016/j.chemgeo.2021.120590.
Makweba, M.M., Holm, E., 1993. The natural radioactivity of the rock phosphates, phosphatic products and their environmental implications. Sci. Total Environ. 133, 99–110. https://doi.org/10.1016/0048-9697(93)90115-M.
Martínez-Aguirre, A., García-León, M., Ivanovich, M., 1994. The distribution of U, Th and 226Ra derived from the phosphate fertilizer industries on an estuarine system in Southwest Spain. J. Environ. Radioact. 22, 155–177. https://doi.org/10.1016/0265-931X(94)90020-5.
McArthur, J.M., Walsh, J.N., 1984. Rare-earth geochemistry of phosphorites. Chem. Geol. 47, 191–220. https://doi.org/10.1016/0009-2541(84)90126-8.
McClellan, G.H., 1980. Mineralogy of carbonate fluorapatites. J. Geol. Soc. Lond. 137, 675–681. https://doi.org/10.1144/gsjgs.137.6.0675.
McClellan, G.H., Van Kauwenbergh, S.J., 1991. Mineralogical and chemical variation of francolites with geological time. JGS 148, 809–812. https://doi.org/10.1144/gsjgs.148.5.0809.
Nance, W.B., Taylor, S.R., 1976. Rare earth element patterns and crustal evolution—I. Australian post-Archean sedimentary rocks. Geochim. Cosmochim. Acta 40, 1539–1551. https://doi.org/10.1016/0016-7037(76)90093-4.
Notholt, A.J.G., Sheldon, R.P., Davidson, D.F., 2005. Phosphate Deposits of the World: Volume 2, Phosphate Rock Resources. Cambridge University Press.
O'Sullivan, G.J., Daly, J.S., Murray, J., Ó'Gogáin, A., Chew, D.M., Drakou, F., Guyett, P. C., Badenszki, E., Hoare, B.C., 2021. Uranium–lead phosphate chronostratigraphy: a proof of concept from the mid-Carboniferous boundary. Sediment. Geol. 422, 105961 https://doi.org/10.1016/j.sedgeo.2021.105961.
Ounis, A., Kocsis, L., Chaabani, F., Pfeifer, H.-R., 2008. Rare earth elements and stable isotope geochemistry (δ13C and δ18O) of phosphorite deposits in the Gafsa Basin, Tunisia. Palaeogeogr. Palaeoclimatol. Palaeoecol. 268, 1–18. https://doi.org/10.1016/j.palaeo.2008.07.005.
Pérez-López, R., Nieto, J.M., López-Coto, I., Aguado, J.L., Bolívar, J.P., Santisteban, M., 2010. Dynamics of contaminants in phosphogypsum of the fertilizer industry of Huelva (SW Spain): from phosphate rock ore to the environment. Appl. Geochem. 25, 705–715. https://doi.org/10.1016/j.apgeochem.2010.02.003.
Picard, S., Lécuyer, C., Barrat, J.-A., Garcia, J.-P., Dromart, G., Sheppard, S.M.F., 2002. Rare earth element contents of Jurassic fish and reptile teeth and their potential relation to seawater composition (Anglo-Paris Basin, France and England). Chem. Geol. 186, 1–16. https://doi.org/10.1016/S0009-2541(01)00424-7.
Pufahl, P.K., Groat, L.A., 2017. Sedimentary and Igneous Phosphate deposits: Formation and Exploration: an Invited Paper. Econ. Geol. 112, 483–516. https://doi.org/10.2113/econgeo.112.3.483.
R Core Team, 2021. R: A Language and Environment for Statistical Computing.
Reynard, B., Lécuyer, C., Grandjean, P., 1999. Crystal-chemical controls on rare-earth element concentrations in fossil biogenic apatites and implications for paleoenvironmental reconstructions. Chem. Geol. 155, 233–241. https://doi.org/10.1016/S0009-2541(98)00169-7.
Roy, S., Négrel, P., 2001. A Pb isotope and trace element study of rainwater from the Massif Central (France). Sci. Total Environ. 277, 225–239. https://doi.org/10.1016/S0048-9697(00)00883-4.
Rutherford, P.M., Dudas, M.J., Samek, R.A., 1994. Environmental impacts of phosphogypsum. Sci. Total Environ. 149, 1–38. https://doi.org/10.1016/0048-9697(94)90002-7.
Rutherford, P.M., Dudas, M.J., Arocena, J.M., 1995. Radioactivity and elemental composition of phosphogypsum produced from three phosphate rock sources. Waste Manag. Res. 13, 407–423. https://doi.org/10.1016/S0734-242X(05)80021-7.
Sangster, D.F., Outridge, P.M., Davis, W.J., 2000. Stable lead isotope characteristics of lead ore deposits of environmental significance. Environ. Rev. 8, 115–147. https://doi.org/10.1139/a00-008.
Sarangi, S., Gopalan, K., Kumar, S., 2004. Pb–Pb age of earliest megascopic, eukaryotic alga bearing Rohtas Formation, Vindhyan Supergroup, India: implications for Precambrian atmospheric oxygen evolution. Precambrian Res. 132, 107–121. https://doi.org/10.1016/j.precamres.2004.02.006.
Sattouf, M., Kratz, S., Diemer, K., Rienitz, O., Fleckenstein, J., Schiel, D., Schnug, E., 2007. Identifying the origin of rock phosphates and phosphorus fertilizers through high-precision measurement of the strontium isotopes 87Sr and 86Sr. Landbauforschung Völkenrode 12.
Sattouf, M., Kratz, S., Diemer, K., Fleckenstein, J., Rienitz, O., Schiel, D., Schnug, E., 2008. Significance of uranium and strontium isotope ratios for retracing the fate of uranium during the processing of phosphate fertilizers from rock phosphates. In: Loads and Fate of Fertilizer Derived Uranium. Backhuys Publishers, Leiden, The Netherlands, pp. 191–202.
Schnug, E., De Kok, L.J. (Eds.), 2016. Phosphorus in Agriculture: 100% Zero. Springer, Netherlands, Dordrecht. https://doi.org/10.1007/978-94-017-7612-7.
Schnug, E., Sun, Y., Zhang, L., Windmann, H., Lottermoser, B.G., Ulrich, A.E., Bol, R., Maekawa, M., Haneklaus, S.H., 2023. Elemental Loads with Phosphate Fertilizers: A Constraint for Soil Productivity?. In: Soil Constraints and Productivity. CRC Press.
Shields, G., Stille, P., 2001. Diagenetic constraints on the use of cerium anomalies as palaeoseawater redox proxies: an isotopic and REE study of Cambrian phosphorites. Chem. Geol., Respon. Ocean. / Atmosph. Syst. Past Glob. Chang. 175, 29–48. https://doi.org/10.1016/S0009-2541(00)00362-4.
Shields, G.A., Webb, G.E., 2004. Has the REE composition of seawater changed over geological time? Chem. Geol. 204, 103–107. https://doi.org/10.1016/j.chemgeo.2003.09.010.
Soudry, D., Glenn, C.R., Nathan, Y., Segal, I., VonderHaar, D., 2006. Evolution of Tethyan phosphogenesis along the northern edges of the Arabian–African shield during the Cretaceous–Eocene as deduced from temporal variations of Ca and Nd isotopes and rates of P accumulation. Earth Sci. Rev. 78, 27–57. https://doi.org/10.1016/j.earscirev.2006.03.005.
Sun, Y., Amelung, W., Wu, B., Haneklaus, S., Maekawa, M., Lücke, A., Schnug, E., Bol, R., 2020. 'Co-evolution' of uranium concentration and oxygen stable isotope in phosphate rocks. Appl. Geochem. 114, 104476 https://doi.org/10.1016/j.apgeochem.2019.104476.
Van Kauwenbergh, S.J., Cathcart, J.B., McClellan, G.H., 1990. Mineralogy and Alteration of the Phosphate Deposits of Florida (No. 1914), Bulletin. U.S. G.P.O.; For sale by the Books and Open-File Reports Section. U.S. Geological Survey. https://doi.org/10.3133/b1914.
Vengosh, A., Wang, Z., Williams, G., Hill, R., Coyte, M.R., Dwyer, G.S., 2022. The strontium isotope fingerprint of phosphate rocks mining. Sci. Total Environ. 850, 157971 https://doi.org/10.1016/j.scitotenv.2022.157971.
Verbeeck, M., Salaets, P., Smolders, E., 2020. Trace element concentrations in mineral phosphate fertilizers used in Europe: a balanced survey. Sci. Total Environ. 712, 136419 https://doi.org/10.1016/j.scitotenv.2019.136419.
Wang, Z., Dwyer, G.S., Coleman, D.S., Vengosh, A., 2019. Lead Isotopes as a New Tracer for Detecting Coal Fly Ash in the Environment. Environ. Sci. Technol. Lett. 6, 714–719. https://doi.org/10.1021/acs.estlett.9b00512.
Wright, J., Schrader, H., Holser, W.T., 1987. Paleoredox variations in ancient oceans recorded by rare earth elements in fossil apatite. Geochim. Cosmochim. Acta 51, 631–644. https://doi.org/10.1016/0016-7037(87)90075-5.
Xin, H., Jiang, S.-Y., Yang, J.-H., Wu, H.-P., Pi, D.-H., 2015. Rare earth element and Sr–Nd isotope geochemistry of phosphatic rocks in Neoproterozoic Ediacaran Doushantuo Formation in Zhangcunping section from western Hubei Province, South China. Palaeogeogr. Palaeoclimatol. Palaeoecol. 440, 712–724. https://doi.org/10.1016/j.palaeo.2015.09.034.
Yang, H., Xiao, J., Xia, Y., Xie, Z., Tan, Q., Xu, J., Guo, H., He, S., Wu, S., 2019. Origin of the Ediacaran Weng'an and Kaiyang phosphorite deposits in the Nanhua basin, SW China. J. Asian Earth Sci. 182, 103931 https://doi.org/10.1016/j.jseaes.2019.103931.
Yang, H., Xiao, J., Xia, Y., Zhao, Z., Xie, Z., He, S., Wu, S., 2022. Diagenesis of Ediacaran – early Cambrian phosphorite: Comparisons with recent phosphate sediments based on LA-ICP-MS and EMPA. Ore Geol. Rev. 144, 104813 https://doi.org/10.1016/j.oregeorev.2022.104813.
Yuan, H., Yuan, W., Cheng, C., Liang, P., Liu, X., Dai, M., Bao, Z., Zong, C., Chen, K., Lai, S., 2016. Evaluation of lead isotope compositions of NIST NBS 981 measured by thermal ionization mass spectrometer and multiple-collector inductively coupled plasma mass spectrometer. Solid Earth Sci. 1, 74–78. https://doi.org/10.1016/j.sesci.2016.04.001.
Zhang, J., Amakawa, H., Nozaki, Y., 1994. The comparative behaviors of yttrium and lanthanides in the seawater of the North Pacific. Geophys. Res. Lett. 21, 2677–2680. https://doi.org/10.1029/94GL02404.